ARTICLE

Bhlhe40 is an essential repressor of IL-10 during *Mycobacterium tuberculosis* infection

Jeremy P. Huynh[1]*, Chih-Chung Lin[2]*, Jacqueline M. Kimmey[1], Nicholas N. Jarjour[2], Elizabeth A. Schwarzkopf[2], Tara R. Bradstreet[2], Irina Shchukina[2], Oleg Shpynov[2,3], Casey T. Weaver[4], Reshma Taneja[5], Maxim N. Artyomov[2], Brian T. Edelson[2], and Christina L. Stallings[1]

The cytokine IL-10 antagonizes pathways that control *Mycobacterium tuberculosis* (*Mtb*) infection. Nevertheless, the impact of IL-10 during *Mtb* infection has been difficult to decipher because loss-of-function studies in animal models have yielded only mild phenotypes. We have discovered that the transcription factor basic helix-loop-helix family member e40 (Bhlhe40) is required to repress *Il10* expression during *Mtb* infection. Loss of Bhlhe40 in mice results in higher *Il10* expression, higher bacterial burden, and early susceptibility similar to that observed in mice lacking IFN-γ. Deletion of *Il10* in *Bhlhe40*^{−/−} mice reverses these phenotypes. Bhlhe40 deletion in T cells or CD11c^{+} cells is sufficient to cause susceptibility to *Mtb*. Bhlhe40 represents the first transcription factor found to be essential during *Mtb* infection to specifically regulate *Il10* expression, revealing the importance of strict control of IL-10 production by innate and adaptive immune cells during infection. Our findings uncover a previously elusive but significant role for IL-10 in *Mtb* pathogenesis.

Introduction

Host immune responses mediate both the disease outcome and the pathology of tuberculosis (TB) caused by *Mycobacterium tuberculosis* (*Mtb)* infection. IFN-γ signaling through the transcription factor STAT1 is essential for the control of mycobacterial infections in humans and mice (Cooper et al., 1993; Flynn et al., 1993; MacMicking et al., 2003; Bustamante et al., 2014). IL-10 is an immunoregulatory cytokine produced by innate and adaptive immune cell types (Gabryšová et al., 2014; Moreira-Teixeira et al., 2017) that antagonizes IFN-γ–associated pathways by suppressing macrophage responsiveness to IFN-γ (Gazzinelli et al., 1992), modulating T-helper (T_H) 1 cell IFN-γ production (Turner et al., 2002; Beamer et al., 2008; Redford et al., 2010), and restricting production of the hallmark T_H1-inducing cytokine IL-12 (Roach et al., 2001; Demangel et al., 2002; Schreiber et al., 2009). IL-10 can also inhibit dendritic cell (DC) migration (Demangel et al., 2002) and limit secretion of myeloid cell–derived proinflammatory cytokines (de Waal Malefyt et al., 1991). Global loss-of-function studies have demonstrated a detrimental role for *Il10* expression in the control of chronic *Mtb* infection in mice, although the magnitude of this effect appears dependent on the genetic background and is generally mild (Roach et al., 2001; Beamer et al., 2008; Redford et al., 2010). More recently, conditional deletion of *Il10* in T cells or CD11c^{+} cells showed that IL-10 production by these two cell types exacerbates *Mtb* infection (Moreira-Teixeira et al., 2017). Overexpression of IL-10 in mice has also supported a negative role for IL-10 in controlling mycobacterial infection, although differences in genetic background, transgenic (Tg) promoters, and mycobacterial species used have resulted in an unclear picture (Murray et al., 1997; Feng et al., 2002; Turner et al., 2002; Schreiber et al., 2009).

Given the potential for IL-10 to negatively impact protective immune responses, cell-intrinsic mechanisms likely exist to regulate IL-10 expression. However, the factors required for this regulation remain poorly understood. *Mtb* directly stimulates IL-10 production from monocytes, macrophages, DCs, and neutrophils via pattern-recognition receptor signaling (Redford et al., 2011). In addition, different T_H cell subsets produce IL-10 in response to distinct combinations of cytokines (Gabryšová et al., 2014). These signals lead to the binding of diverse transcription factors at various promoter and enhancer elements within the *Il10* locus to activate transcription within myeloid and lymphoid cells (Saraiva and O'Garra, 2010; Gabryšová et al., 2014; Hörber et al., 2016). Much less is known about transcriptional pathways that limit the production of IL-10 (Iyer and Cheng, 2012). In this study, we report that the transcription factor basic helix-loop-helix family member e40 (Bhlhe40) serves an essential role in resistance to *Mtb* infection by repressing *Il10* expression in both T cells and myeloid cells.

[1]Department of Molecular Microbiology, Washington University School of Medicine, St. Louis, MO; [2]Department of Pathology and Immunology, Washington University School of Medicine, St. Louis, MO; [3]JetBrains Research, Saint Petersburg, Russia; [4]Department of Pathology, University of Alabama at Birmingham, Birmingham, AL; [5]Department of Physiology, Yong Loo Lin School of Medicine, National University of Singapore, Singapore.

*J.P. Huynh and C.-C. Lin contributed equally to this paper;   Correspondence to Christina L. Stallings: stallings@wustl.edu;   Brian T. Edelson: bedelson@path.wustl.edu.

Check for updates

Results

Bhlhe40 is required to control *Mtb* infection

We have previously shown that the transcription factor Bhlhe40 regulates cytokine production by T cells in a mouse model of multiple sclerosis (Lin et al., 2014, 2016). When we analyzed publicly available whole-blood gene expression datasets (Berry et al., 2010; Maertzdorf et al., 2011; Bloom et al., 2013), we found that *BHLHE40* transcripts were present at a significantly lower abundance in patients with active TB as compared with healthy controls, those with latent TB infection, or those with lung cancer, pneumonia, or sarcoidosis (Fig. 1 A). This expression pattern contrasted with that of *STAT1*, whose expression was significantly increased in patients with active TB (Fig. 1 A) as previously noted (Berry et al., 2010; Bloom et al., 2013). This finding of decreased *BHLHE40* expression in patients with active TB led us to investigate a role for this transcription factor during *Mtb* infection in mice. We infected *Bhlhe40*^{+/+}, *Bhlhe40*^{+/−}, and *Bhlhe40*^{−/−} mice on the C57BL/6 background with the *Mtb* Erdman strain and monitored morbidity and mortality. *Bhlhe40*^{+/+} and *Bhlhe40*^{+/−} mice displayed no signs of morbidity and survived beyond 100 d postinfection (dpi). *Bhlhe40*^{−/−} mice began losing weight at ∼21 dpi and succumbed to infection between 32 and 40 dpi with a median survival time of 33 d (Fig. 1, B and C). This severe susceptibility phenotype is similar to that of mice lacking STAT1 (MacMicking et al., 2003) and is more severe than that of mice lacking NF-κB p50 (Yamada et al., 2001), both of which are central transcriptional regulators of the immune system. By 21 dpi, *Mtb* CFUs in *Bhlhe40*^{−/−} mice were 23-fold higher in the lung and fivefold higher in the spleen as compared with *Bhlhe40*^{+/+} mice (Fig. 1, D and E). The differences in *Mtb* CFUs in both organs became even more pronounced at 28 dpi, demonstrating an ongoing defect in the ability of *Bhlhe40*^{−/−} mice to control *Mtb* replication. Upon infection with the intracellular bacterium *Listeria monocytogenes*, *Bhlhe40*^{−/−} mice showed no increased susceptibility (Fig. 1, F and G) and mounted a robust response to secondary *L. monocytogenes* challenge (Fig. 1 G), indicating that their susceptibility to *Mtb* was caused by an impaired response specific to this pathogen.

Bhlhe40 deficiency leads to neutrophil-dominated inflammation

Shortly before succumbing to infection, it was evident by gross examination that *Bhlhe40*^{−/−} lungs had developed larger lesions than *Bhlhe40*^{+/+} lungs (Fig. 2 A). Histological analysis confirmed that although there were no differences in pulmonary inflammation before infection, the lungs of *Bhlhe40*^{−/−} mice had developed larger neutrophil- and acid-fast bacilli-rich lesions with more widespread inflammation than *Bhlhe40*^{+/+} lungs by 21 dpi (Figs. 2 B and S1 A). We analyzed these differences further by performing flow cytometry on the immune cell populations present in the lungs of mice before and after *Mtb* infection. By 21 dpi, neutrophils were the predominant CD45^{+} cell type in the lungs of *Bhlhe40*^{−/−} mice, and the absolute number of neutrophils in *Bhlhe40*^{−/−} lungs was three times greater than in *Bhlhe40*^{+/+} lungs (Fig. 2, C and D). The number and frequency of neutrophils in the lungs of *Bhlhe40*^{−/−} mice further increased as the infection progressed (Fig. 2, C and D). The number of CD11b^{+}Ly6C^{high} monocyte-derived DCs (moDCs) was 12-fold lower in *Bhlhe40*^{−/−} mice

at 21 dpi, suggesting that Bhlhe40 may regulate the development, recruitment, or survival of this population (Fig. S1 B). There were no significant differences in the populations sizes of other myeloid or lymphoid cell types analyzed at 21 dpi (Fig. S1 B), nor were there any differences in the frequency of *Mtb* antigen-specific T cells in the lungs or mediastinal lymph nodes (Fig. S1 C).

The timing of the increased inflammation correlated with our initial observation of higher *Mtb* burden in the lungs of *Bhlhe40*^{−/−} mice, leading us to investigate whether the accumulating myeloid cells were infected with *Mtb*. We infected *Bhlhe40*^{+/+} and *Bhlhe40*^{−/−} mice with a strain of *Mtb* Erdman that stably expresses GFP and monitored the number and frequency of *Mtb*-infected cells at 21 dpi. Neutrophils, CD11b^{+} macrophages, inflammatory monocytes, moDCs, and CD11b^{+} DCs were all infected at a higher frequency in *Bhlhe40*^{−/−} lungs compared with *Bhlhe40*^{+/+} lungs (Fig. 2, E and F). Absolute numbers of infected neutrophils, inflammatory monocytes, and CD11b^{+} DCs were also significantly higher in *Bhlhe40*^{−/−} lungs (Fig. S1 D), suggesting that *Mtb* residing within these cell types accounts for the difference in pulmonary *Mtb* burden in *Bhlhe40*^{−/−} lungs at 21 dpi. Infected *Bhlhe40*^{−/−} neutrophils, inflammatory monocytes, moDCs, and CD11b^{+} DCs also exhibited an increase in mean fluorescence intensity (MFI) for GFP compared with infected *Bhlhe40*^{+/+} neutrophils, suggesting that they harbored more *Mtb* on a per-cell basis (Fig. S1 E).

To test whether the influx of neutrophils contributed to the susceptibility of *Bhlhe40*^{−/−} mice, we used an anti-Ly6G monoclonal antibody to specifically deplete neutrophils between 10 and 30 dpi (Kimmey et al., 2015). Neutrophil-depleted *Bhlhe40*^{−/−} mice did not exhibit any improvements in morbidity, survival time, or control of *Mtb* replication (Fig. S1, F–H). Therefore, although neutrophils serve as a prominent replicative niche for *Mtb*, they are not the sole cause of susceptibility to *Mtb* infection in *Bhlhe40*^{−/−} mice.

Bhlhe40 functions in innate and adaptive immune cells

Bhlhe40 is expressed in specific immune cell populations and in nonhematopoietic tissues (Ow et al., 2014). To dissect which cells required Bhlhe40 expression during *Mtb* infection, we first generated reciprocal and control bone marrow chimeric mice, infected them with *Mtb*, and monitored for survival (Fig. 3 A). As expected, all but one *Bhlhe40*^{+/+}→*Bhlhe40*^{+/+} chimeric mouse survived beyond 100 dpi, and *Bhlhe40*^{−/−}→*Bhlhe40*^{−/−} chimeras succumbed between 27 and 35 dpi (median survival time of 33 d). *Bhlhe40*^{+/+}→*Bhlhe40*^{−/−} chimeras also survived past 100 dpi, whereas *Bhlhe40*^{−/−}→*Bhlhe40*^{+/+} chimeras died between 29 and 37 dpi (median survival time of 32 d), similar to the *Bhlhe40*^{−/−}→*Bhlhe40*^{−/−} chimeras. These data demonstrate a specific role for Bhlhe40 in radiosensitive hematopoietic cells during *Mtb* infection.

To determine which hematopoietic cells express Bhlhe40 during *Mtb* infection, we used Bhlhe40-GFP reporter mice (*Bhlhe40*[GFP]; Schmidt et al., 2013; Lin et al., 2016). We monitored GFP expression as a proxy for Bhlhe40 expression in the lungs of naive and *Mtb*-infected *Bhlhe40*[GFP] mice. Sizeable fractions of neutrophils, alveolar macrophages, CD11b^{+} DCs, CD103^{+} DCs, and eosinophils expressed GFP both before infection and at 21 dpi

Huynh et al.
Bhlhe40 represses IL-10 during *M. tuberculosis* infection

Journal of Experimental Medicine
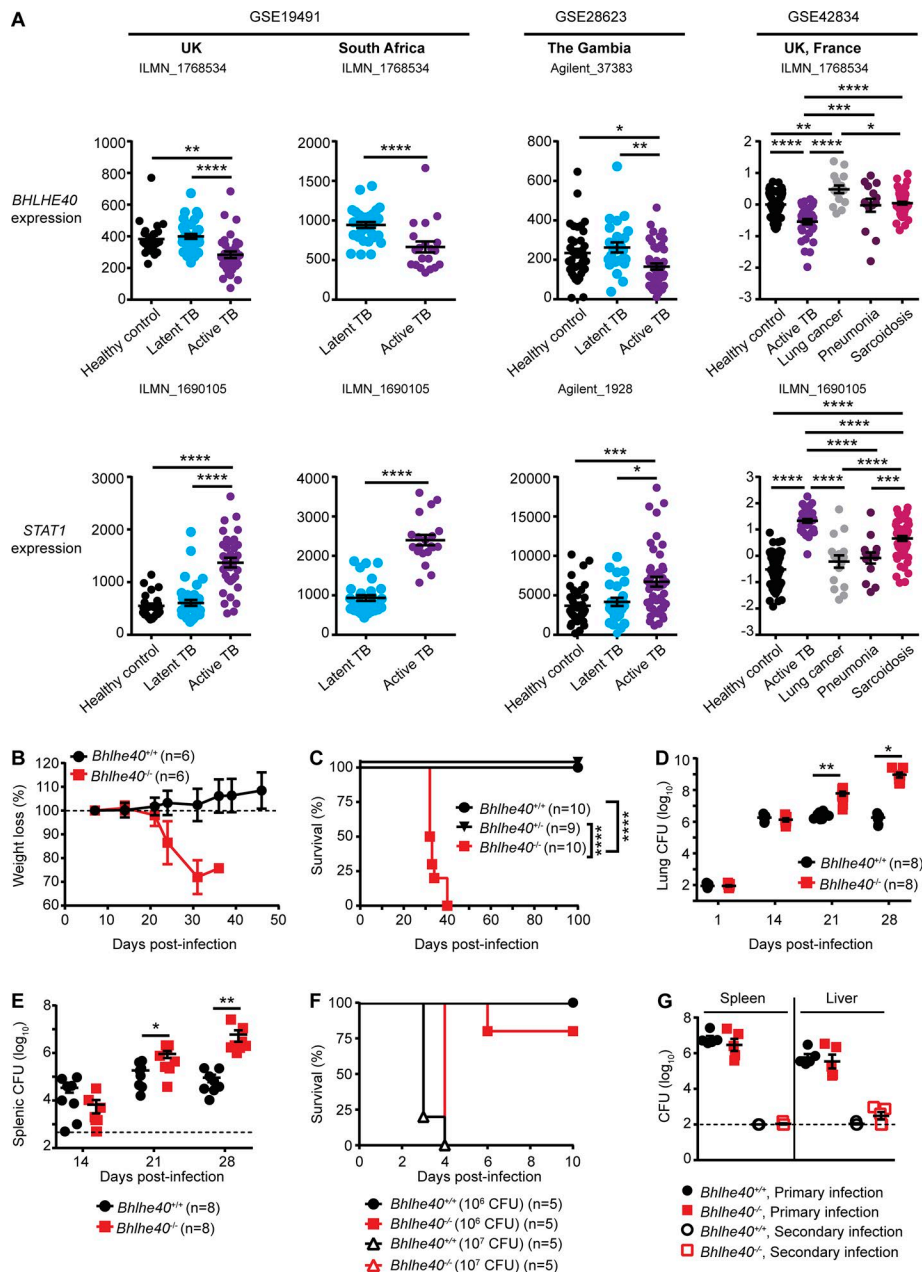https://doi.org/10.1084/jem.20171704

1824

Figure 1. **Bhlhe40 is required to control *Mtb* infection in mice. (A)** Expression of *BHLHE40* and *STAT1* in human whole blood in healthy controls or patients with latent TB, active TB, or other lung diseases. Data are derived from the analysis of the indicated publicly available GEO datasets using the indicated probe sets. **(B–E)** *Bhlhe40+/+*, *Bhlhe40+/−*, and *Bhlhe40−/−* mice were infected with 100–200 CFU aerosolized *Mtb* and monitored for body weight (B; *n* = 6 per group), survival (C; *n* = 9–10 per group), pulmonary *Mtb* burden (D; *n* = 8 per group), and splenic *Mtb* burden (E; *n* = 8 per group). **(F)** Mice were infected with 10^6 or 10^7 CFU of *L. monocytogenes* i.v. and monitored for survival (*n* = 5 per group). **(G)** Mice were infected with 10^6 CFU i.v., and *L. monocytogenes* burden in the spleen and liver was assessed at 3 d after primary or secondary infection (*n* = 5 per group). The dotted lines in E and G indicate limits of detection (500 [E] and 100 [G] CFU). Each point represents data from one human or mouse. The mean ± SEM is graphed. Statistical differences were determined by two-tailed unpaired Student's *t* test, unpaired one-way ANOVA, or unpaired Kruskal-Wallis test (A), log-rank Mantel-Cox test (C and F), and two-tailed unpaired Student's *t* test for normally distributed groups or two-tailed unpaired Mann-Whitney test for nonnormally distributed groups (D, E, and G). *, P < 0.05; **, P < 0.01; ***, P < 0.001; ****, P < 0.0001. Data are from one (F and G) or two independent experiments (B–E).

(Fig. S2), with smaller fractions of CD11b+ macrophages, moDCs, B cells, and CD8+ T cells also showing this pattern of expression. Therefore, these cell types constitutively express Bhlhe40, and this expression pattern does not change during *Mtb* infection. In contrast, CD4+ T cells in naive mice expressed very little Bhlhe40, but at 21 dpi, Bhlhe40 levels increased in this cell type (Fig. S2). These data show that Bhlhe40 is expressed in both myeloid and lymphoid cells during *Mtb* infection.

Bhlhe40 expression is required in CD4+ T cells to regulate cytokine production in the experimental autoimmune encephalomyelitis (EAE) model of autoimmunity (Martínez-Llordella et al., 2013; Lin et al., 2014). However, *Bhlhe40−/−* mice succumbed to *Mtb* infection between 32 and 40 dpi, which is earlier than *Rag1−/−* mice that lack mature B and T cell and that succumb to *Mtb* infection between 46 and 50 dpi (Nandi and Behar, 2011). The timing of the death of *Mtb*-infected *Bhlhe40−/−* mice suggests

that there is a defect in the innate immune response to *Mtb*, as it preceded the point at which adaptive immunity is required, or the presence of pathological T cells is leading to earlier death than would occur in the absence of T cells, as previously observed in *Pdcd1−/−* mice (Barber et al., 2011).

To measure the contribution of Bhlhe40 to host resistance in the absence of mature B and T cells, we compared the survival of *Mtb*-infected *Bhlhe40+/+*, *Bhlhe40−/−*, *Rag1−/−*, and *Rag1−/−Bhlhe40−/−* mice. *Rag1−/−Bhlhe40−/−* mice (median survival time of 33 d) were significantly more susceptible than *Rag1−/−* mice (median survival time of 43 d) to *Mtb* infection and succumbed to infection at the same time as *Bhlhe40−/−* mice (Fig. 3 B). These data demonstrate that Bhlhe40 is required during the innate immune response in the absence of T cells to prolong survival during *Mtb* infection. *Mtb* CFUs were fourfold higher in *Rag1−/−Bhlhe40−/−* mice compared with *Rag1−/−* mice at 21
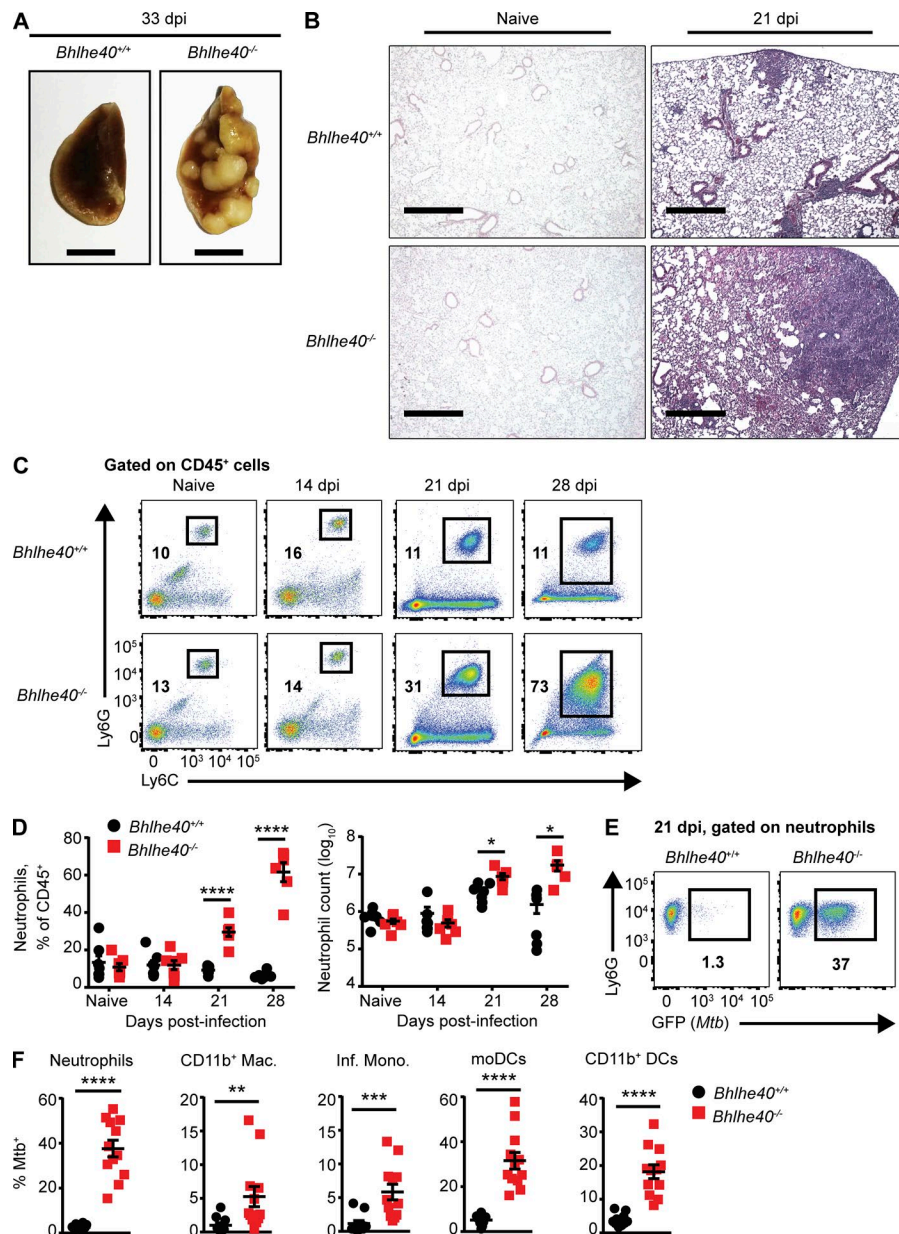
Figure 2. **Bhlhe40 deficiency leads to a neutrophil-dominated inflammatory response and high frequencies of infected myeloid cells.** **(A)** Pulmonary gross pathology was assessed at 33 dpi. Bars, 5 mm. **(B)** Histopathology was visualized by H&E staining of lungs before infection or at 21 dpi. Images shown are at 4× magnification and are representative of two independent experiments with three biological replicates per experiment. Bars, 500 μm. **(C)** Representative flow cytometry plots for neutrophils as a percentage of the total CD45+ population in *Bhlhe40*+/+ or *Bhlhe40*−/− lungs before infection and at 14, 21, and 28 dpi. **(D)** Absolute count and percentage of the total CD45+ population for neutrophils in *Bhlhe40*+/+ and *Bhlhe40*−/− lungs before infection (*n* = 7 per group) and at 14 (*n* = 7 per group), 21 (*n* = 7 per group), and 28 dpi (*n* = 6 per group). **(E)** Representative flow cytometry plots for GFP (*Mtb*)–positive neutrophils in *Bhlhe40*+/+ and *Bhlhe40*−/− lungs at 21 dpi. **(F)** Frequency of GFP (*Mtb*)–positive cells in *Bhlhe40*+/+ and *Bhlhe40*−/− myeloid lung populations at 21 dpi (*n* = 10–12 per group). Mac., macrophage; Inf. Mono., inflammatory monocyte. **(D and F)** Each point represents data from one mouse. The mean ± SEM is graphed. Statistical differences were determined by two-tailed unpaired Student's *t* test for normally distributed groups or two-tailed unpaired Mann-Whitney test for nonnormally distributed groups as appropriate. *, P < 0.05; **, P < 0.01; ***, P < 0.001; ****, P < 0.0001. Data are from or representative of two (A–D) or five (E and F) independent experiments.

dpi (Fig. 3 C), and the frequency of neutrophils in the lungs of *Rag1*−/−*Bhlhe40*−/− mice was also significantly elevated (Fig. S3 A). The frequency of infected neutrophils, CD11b+ macrophages, and moDCs was significantly higher in *Rag1*−/−*Bhlhe40*−/− mice at 21 dpi (Fig. S3 B). We also observed significantly higher MFIs for GFP in *Rag1*−/−*Bhlhe40*−/− neutrophils, CD11b+ macrophages, inflammatory monocytes, and CD11b+ DCs, suggesting that these cell types harbored more *Mtb* on a per-cell basis compared with *Rag1*−/− cells (Fig. S3 C). Therefore, loss of Bhlhe40 in innate immune cells compromises their ability to control inflammation and *Mtb* replication independent of adaptive immunity.

To determine more precisely which cells require Bhlhe40 expression to control *Mtb* infection, we infected mice that conditionally delete *Bhlhe40* in specific cell types. After *Mtb* infection, *Bhlhe40*fl/fl-*Lysm-Cre* and *Bhlhe40*fl/fl-*Mrp8-Cre* mice showed no signs of morbidity (Fig. S3 D) and survived past 100 dpi (Fig. 3 D), indicating that loss of Bhlhe40 in LysM+ or Mrp8+ cells was not

sufficient to generate susceptibility to infection. In contrast, *Bhlhe40*fl/fl-*Cd11c-Cre* and *Bhlhe40*fl/fl-*Cd4-Cre* mice succumbed to infection at 34–62 d (median survival time of 56 d) and 31–73 d (median survival time of 52 d), respectively (Fig. 3 D). Therefore, Bhlhe40 expression in both T cells and CD11c+ cells is required to control *Mtb* infection. Given that the *Lysm* promoter can drive conditional deletion in alveolar macrophages but deletes poorly in myeloid DCs, whereas the *Cd11c* promoter deletes equally well in both alveolar macrophages and DCs (Abram et al., 2014), one interpretation is that loss of Bhlhe40 in alveolar macrophages is not sufficient to cause susceptibility and that loss of Bhlhe40 in DCs contributes to the susceptibility observed in *Bhlhe40*fl/fl-*Cd11c-Cre* mice.

We next analyzed susceptible *Bhlhe40*fl/fl-*Cd4-Cre* and *Bhlhe40*fl/fl-*Cd11c-Cre* mice to determine how loss of Bhlhe40 in CD11c+ or T cells contributed to phenotypes observed in *Bhlhe40*−/− mice. By 21 dpi, pulmonary *Mtb* burden in *Bhlhe40*fl/fl-

Huynh et al.
Bhlhe40 represses IL-10 during *M. tuberculosis* infection

Journal of Experimental Medicine
https://doi.org/10.1084/jem.20171704

1826

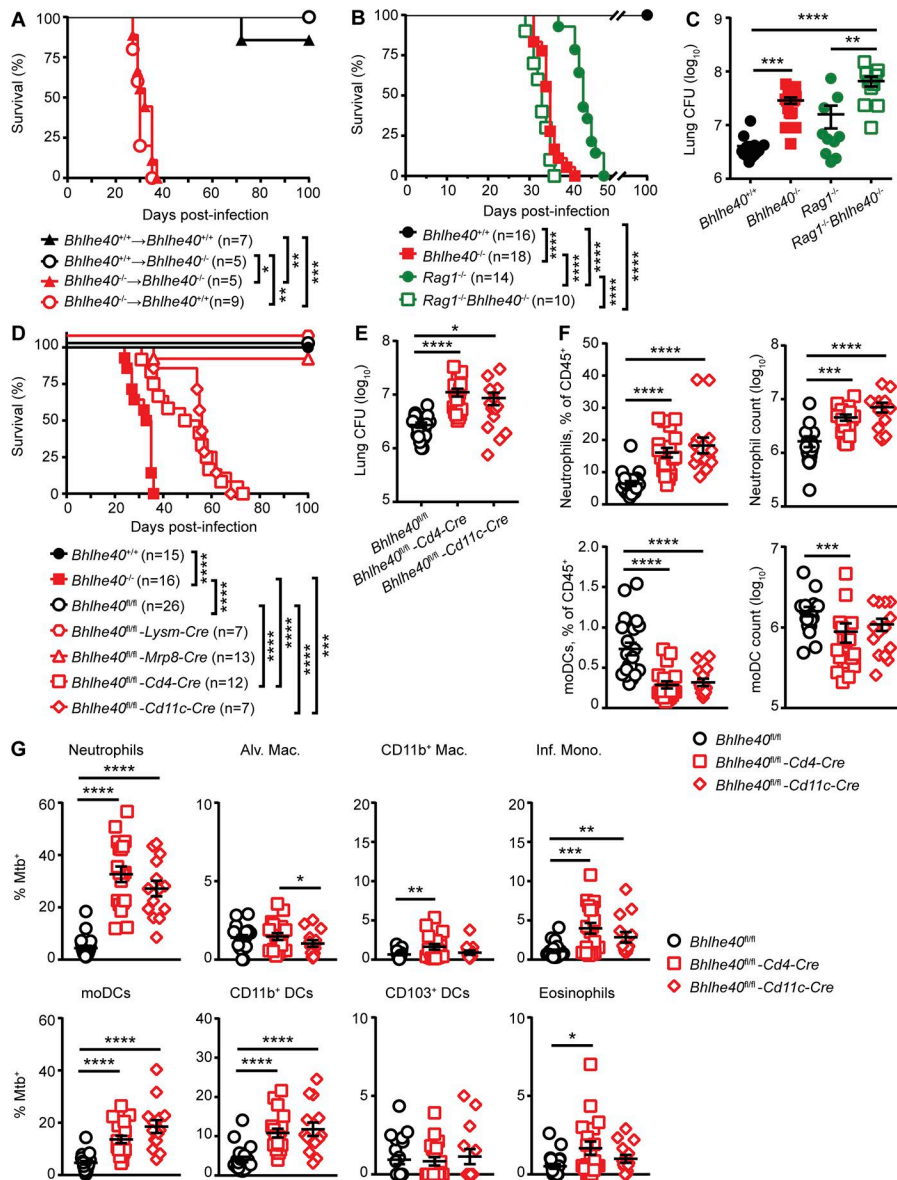**Figure 3. Bhlhe40 functions in both innate and adaptive immune cells to control *Mtb* infection. (A)** *Bhlhe40⁺/⁺* or *Bhlhe40⁻/⁻* mice were lethally irradiated, reconstituted with *Bhlhe40⁺/⁺* or *Bhlhe40⁻/⁻* bone marrow, and monitored for survival after *Mtb* infection (n = 5–9 per group). **(B and C)** *Bhlhe40⁺/⁺*, *Bhlhe40⁻/⁻*, *Rag1⁻/⁻*, or *Rag1⁻/⁻ Bhlhe40⁻/⁻* mice were infected with *Mtb* and monitored for survival (B; n = 10–18 per group) or lung *Mtb* burden at 21 dpi (C; n = 10–17 per group). **(D–G)** *Bhlhe40⁺/⁺*, *Bhlhe40⁻/⁻*, *Bhlhe40^fl/fl*, *Bhlhe40^fl/fl-Lysm-Cre*, *Bhlhe40^fl/fl-Mrp8-Cre*, *Bhlhe40^fl/fl-Cd4-Cre*, and *Bhlhe40^fl/fl-Cd11c-Cre* mice were infected with *Mtb* and monitored for survival (D; n = 7–26 per group), lung *Mtb* burden at 21 dpi (E; n = 14–21 per group), lung neutrophil and moDC absolute count along with percentage of the total CD45⁺ population at 21 dpi (F; n = 14–21 per group), and frequency of GFP (*Mtb*)–positive lung cells at 21 dpi (G; n = 14–21 per group). Mac., macrophage; Inf. Mono., inflammatory monocyte; Alv. Mac., alveolar macrophage. **(A, B, and D)** Each point represents data from one mouse, and the mean ± SEM is shown. The number of biological replicates is indicated in parentheses. Statistical differences were determined by log-rank Mantel-Cox test. In D, *Bhlhe40^fl/fl-Cd4-Cre* and *Bhlhe40^fl/fl-Cd11c-Cre* mice were compared with *Bhlhe40^fl/fl*, *Bhlhe40⁻/⁻*, and each other. **(C, E, and G)** Statistical differences were determined by one-way unpaired ANOVA with Tukey's post test for normally distributed groups or unpaired Kruskal-Wallis test with Dunn's multiple comparison test for nonnormally distributed groups. *, P < 0.05; **, P < 0.01; ***, P < 0.001; ****, P < 0.0001. Data are from two (A), four (B), five (C), or seven (D–G) independent experiments.

Cd4-Cre and *Bhlhe40^fl/fl-Cd11c-Cre* mice was four- and threefold higher than *Bhlhe40^fl/fl* controls, respectively (Fig. 3 E). *Bhlhe40^fl/fl-Cd4-Cre* and *Bhlhe40^fl/fl-Cd11c-Cre* mice also exhibited an increase in the frequency and absolute number of pulmonary neutrophils (Fig. 3 F). The frequency of moDCs was significantly lower in *Bhlhe40^fl/fl-Cd4-Cre* and *Bhlhe40^fl/fl-Cd11c-Cre* lungs, but the absolute number of moDCs was decreased in *Bhlhe40^fl/fl-Cd4-Cre* lungs only, suggesting that loss of Bhlhe40 in T cells leads to the decreased number of moDCs observed in *Bhlhe40⁻/⁻* mice (Figs. 3 F and S1 B). Neutrophils, inflammatory monocytes, moDCs, and CD11b⁺ DCs were infected at a higher frequency in both *Bhlhe40^fl/fl-Cd4-Cre* and *Bhlhe40^fl/fl-Cd11c-Cre* mice (Fig. 3 G). Although survival, *Mtb* burden, neutrophilic inflammation, and frequency of cellular infection phenotypes were evident in *Bhlhe40^fl/fl-Cd4-Cre* and *Bhlhe40^fl/fl-Cd11c-Cre* mice, they were less severe than in *Bhlhe40⁻/⁻* mice, suggesting that defects caused by Bhlhe40 deficiency in CD11c⁺ cells, T cells, and potentially other cell types combine to undermine protective responses to *Mtb*.

Bhlhe40 represses IL-10 production after exposure to *Mtb*

Bhlhe40 has previously been found to regulate cytokine production by CD4⁺ T cells in the EAE model (Martínez-Llordella et al., 2013; Lin et al., 2014). If Bhlhe40 functions analogously during *Mtb* infection, *Bhlhe40⁻/⁻* cells could exert a dominant effect on *Bhlhe40⁺/⁺* cells through the production of secreted cytokines. We tested this by generating mixed bone marrow chimeric mice. Congenically marked *Bhlhe40⁺/⁺* (CD45.1/.2) recipients were lethally irradiated and reconstituted with a 1:1 mixture of *Bhlhe40⁺/⁺* (CD45.1/.1) and *Bhlhe40⁻/⁻* (CD45.2/.2) bone marrow cells. Control mice included mixed chimeras generated with *Bhlhe40⁺/⁺* (CD45.1/.1) and *Bhlhe40⁺/⁺* (CD45.2/.2) bone marrow cells as well as nonchimeric *Bhlhe40⁺/⁺* (CD45.2/.2) and *Bhlhe40⁻/⁻* (CD45.2/.2) mice. In mixed chimeras, *Bhlhe40⁻/⁻* bone marrow cells were capable of normal reconstitution of the hematopoietic compartment within the lung (Fig. 4 A). Chimeric mice were infected with GFP-expressing *Mtb* and analyzed at 21 dpi. *Bhlhe40⁺/⁺ + Bhlhe40⁺/⁺* chimeras controlled *Mtb* infection with little neutrophilic infiltrate (unpublished data) and a low

Huynh et al.
Bhlhe40 represses IL-10 during *M. tuberculosis* infection

Journal of Experimental Medicine
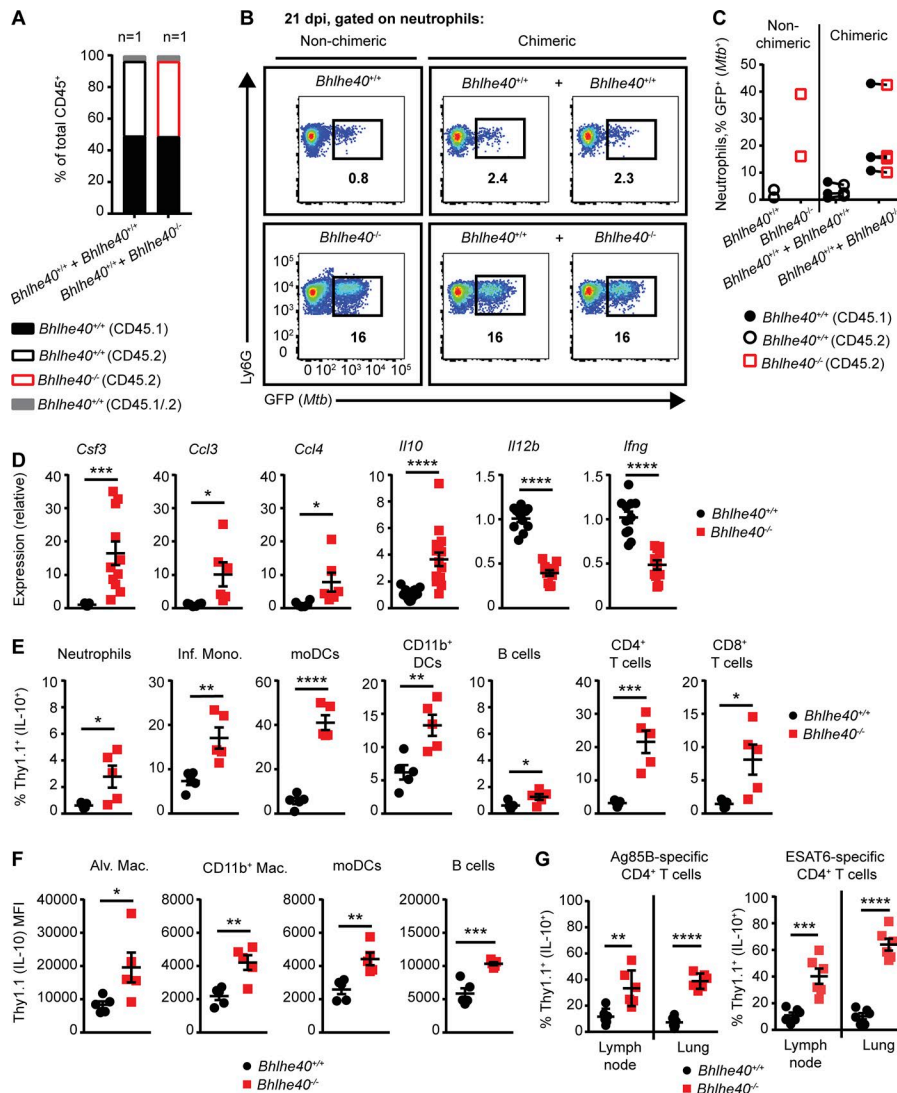https://doi.org/10.1084/jem.20171704

1827

Figure 4. **Multiple immune cells require Bhlhe40 to repress IL-10 production after exposure to *Mtb*. (A)** The frequency of CD45.1⁺, CD45.2⁺, and CD45.1⁺CD45.2⁺ lung cells in naive mixed bone marrow chimeric mice (n = 1 per group). **(B and C)** Representative flow cytometry plots (B) and frequency of infected neutrophils in the lungs of nonchimeric and mixed bone marrow chimeric mice infected with GFP-*Mtb* at 21 dpi (C; n = 2–4 per group). **(D)** Cytokine transcript levels were assessed at 21 dpi in total lung samples from *Bhlhe40*⁺/⁺ and *Bhlhe40*⁻/⁻ mice (n = 11 or 16 per group). **(E)** The frequency of Thy1.1 (IL-10)–expressing immune cells in 10BiT⁺ *Bhlhe40*⁺/⁺ and *Bhlhe40*⁻/⁻ lungs at 21 dpi (n = 5 per group). **(F)** Geometric MFI for FITC (Thy1.1 [IL-10]) on Thy1.1-expressing lung cells at 21 dpi (n = 5 per group). Mac., macrophage; Inf. Mono., inflammatory monocyte; Alv. Mac., alveolar macrophage. **(G)** Thy1.1-expressing Ag85B- or ESAT6-specific CD4⁺ T cells as a percentage of the total Ag85B- or ESAT6-specific CD4⁺ T cell population in the lungs or mediastinal lymph nodes of 10BiT⁺ *Bhlhe40*⁺/⁺ or *Bhlhe40*⁻/⁻ mice at 21 dpi (n = 6 per group). Each point represents data from one mouse except in C, where data from the same mouse is connected by a line. The mean ± SEM is graphed. Statistical differences were determined by two-tailed unpaired Student's *t* test for normally distributed groups or two-tailed unpaired Mann-Whitney test for nonnormally distributed groups. *, P < 0.05; **, P < 0.01; ***, P < 0.001; ****, P < 0.0001. Data are from one (A) or two (B–G) independent experiments.

frequency of neutrophil infection (Fig. 4, B and C). Lungs of mixed *Bhlhe40*⁺/⁺ + *Bhlhe40*⁻/⁻ chimeras contained large populations of infiltrating neutrophils of both genotypes (unpublished data). Neutrophils of both genotypes displayed a high frequency of *Mtb* infection (Fig. 4, B and C), which correlated with a trend toward higher CFUs in the lungs of mixed *Bhlhe40*⁺/⁺ + *Bhlhe40*⁻/⁻ chimeras (Fig. S3 E). These results demonstrate that *Bhlhe40*⁻/⁻ cells, even when present as only half of all hematopoietic cells, exert a dominant influence in trans on the ability of *Bhlhe40*⁺/⁺ cells to control neutrophil accumulation and *Mtb* infection.

These data indicate that Bhlhe40 likely regulates secreted factors such as cytokines or chemokines, which can impact other cells. Therefore, we analyzed cytokine and chemokine levels in total lung samples from *Bhlhe40*⁺/⁺ and *Bhlhe40*⁻/⁻ mice by quantitative RT-PCR. At 21 dpi, transcripts for the neutrophil-associated cytokines *Csf3* (G-CSF), *Ccl3* (MIP-1α), and *Ccl4* (MIP-1β) were up-regulated in *Bhlhe40*⁻/⁻ lungs (Fig. 4 D) as expected given the neutrophil-dominated inflammation observed. We also found that at 21 dpi, *Il10* (IL-10) transcript levels were three-fold higher in *Bhlhe40*⁻/⁻ lungs, and *Il12b* (IL-12/23p40) and *Ifng* (IFN-γ) transcript levels were three- and twofold lower in

Bhlhe40⁻/⁻ lungs, respectively, compared with *Bhlhe40*⁺/⁺ lungs (Fig. 4 D). This finding was of particular interest because Bhlhe40 represses *Il10* transcription in CD4⁺ T cells in the EAE model (Lin et al., 2014) and IL-10 has been shown to inhibit IL-12/23p40 and IFN-γ expression during *Mtb* infection (Roach et al., 2001; Turner et al., 2002; Schreiber et al., 2009; Redford et al., 2010). In the lungs of naive *Bhlhe40*⁺/⁺ and *Bhlhe40*⁻/⁻ mice, there were no differences in the levels of *Ifng* and *Csf3* transcript, and *Il10* and *Il12b* transcript levels were below the level of detection (unpublished data), indicating that loss of Bhlhe40 impacts expression of these genes during *Mtb* infection but not in naive mice.

The increased *Il10* transcript levels in conjunction with decreased *Il12b* and *Ifng* transcript levels in *Bhlhe40*⁻/⁻ lungs at 21 dpi indicated that Bhlhe40 could be regulating *Il10* expression. To identify the cell types responsible for the increased *Il10* expression in *Bhlhe40*⁻/⁻ lungs, we used Tg *Il10* bacterial artificial chromosome (BAC)-in transgene (10BiT) IL-10 reporter mice (Maynard et al., 2007), where *Il10*-expressing cells display Thy1.1 on their surface. We observed a similar distribution of *Il10*-expressing cells in 10BiT⁺ *Bhlhe40*⁺/⁺ mice as reported in a recent study that used these reporter mice to characterize

Huynh et al.
Bhlhe40 represses IL-10 during *M. tuberculosis* infection

Journal of Experimental Medicine
https://doi.org/10.1084/jem.20171704

1828

sources of IL-10 before and after *Mtb* infection (Moreira-Teixeira et al., 2017). We crossed 10BiT and *Bhlhe40*$^{-/-}$ mice to generate a *Bhlhe40*$^{-/-}$ 10BiT-positive strain, and then we analyzed Thy1.1 expression as a proxy for *Il10* expression. We observed low levels of Thy1.1 expression in naive 10BiT$^+$ *Bhlhe40*$^{+/+}$ and 10BiT$^+$ *Bhlhe40*$^{-/-}$ mice (Fig. S4 A). At 21 dpi, no differences were observed when comparing the absolute number of Thy1.1$^+$ cells, but the frequency of Thy1.1$^+$ neutrophils, inflammatory monocytes, moDCs, CD11b$^+$ DCs, B cells, CD4$^+$ T cells, and CD8$^+$ T cells was significantly higher in *Bhlhe40*$^{-/-}$ mice (Figs. 4 E and S4, B and C). In addition, when we compared the MFIs for Thy1.1 on Thy1.1$^+$ cells, we found that not only were a higher percentage of *Bhlhe40*$^{-/-}$ moDCs and B cells expressing Thy1.1, but these cell types also expressed more Thy1.1 on a per-cell basis during *Mtb* infection (Fig. 4 F). Significantly higher Thy1.1 MFI was also observed on *Bhlhe40*$^{-/-}$ Thy1.1$^+$ alveolar macrophages and CD11b$^+$ macrophages (Fig. 4 F). The increased frequency of Thy1.1 positivity observed in *Bhlhe40*$^{-/-}$ CD4$^+$ T cells was even more pronounced in *Bhlhe40*$^{-/-}$ *Mtb*–specific CD4$^+$ T cells in the mediastinal lymph node and lung, indicating that *Mtb*-specific CD4$^+$ T cells take on an immunosuppressive phenotype in the absence of Bhlhe40 (Fig. 4 G). These data demonstrated that the frequency and per-cell expression of *Il10* was increased in multiple *Bhlhe40*$^{-/-}$ myeloid and lymphoid populations.

Bhlhe40 suppresses IL-10 expression in myeloid cells in vitro

We sought to identify an in vitro myeloid cell culture system that recapitulates the effects of Bhlhe40 deficiency on IL-10 production in response to *Mtb*. We cultured *Bhlhe40*$^{+/+}$ bone marrow cells with GM-CSF or macrophage CSF (M-CSF) and determined by Western blot analysis that only cells cultured with GM-CSF, which comprise a mixture of granulocytes, macrophage-like cells, and DC-like cells (Helft et al., 2015; Poon et al., 2015), express Bhlhe40 (Fig. 5 A). Analysis of GM-CSF– and M-CSF–cultured cells from *Bhlhe40*^{GFP} reporter mouse bone marrow confirmed that only GM-CSF–cultured bone marrow–derived cells expressed GFP (Fig. 5 B). This expression of *Bhlhe40* in granulocytes, macrophage-like cells, and DC-like cells cultured with GM-CSF may relate to the expression of Bhlhe40 by these cell types in the lung (Fig. S2; Heng et al., 2008; Lin et al., 2016), where GM-CSF is abundant and plays an important part in the development and function of lung myeloid cells (Kopf et al., 2015). Loss of Bhlhe40 did not significantly affect the ability of GM-CSF–cultured cells to control *Mtb* replication in the presence or absence of IFN-γ (Fig. S5 A), suggesting that Bhlhe40 is dispensable for the ability of these cell types to control *Mtb* replication.

We next assessed IL-10 expression from *Bhlhe40*$^{+/+}$ and *Bhlhe40*$^{-/-}$ cells cultured with GM-CSF. In the absence of stimulation with heat-killed *Mtb*, minimal IL-10 protein was detected in culture supernatants (Fig. 5 C). In contrast, *Bhlhe40*$^{-/-}$ GM-CSF–cultured bone marrow–derived cells stimulated with heat-killed *Mtb* for 24 h produced significantly more IL-10 than *Bhlhe40*$^{+/+}$ cells (Fig. 5 C). We also stimulated 10BiT$^+$ *Bhlhe40*$^{+/+}$ and *Bhlhe40*$^{-/-}$ GM-CSF–cultured cells with heat-killed *Mtb*, assessed Thy1.1 expression by flow cytometry, and measured IL-10 in culture supernatants by ELISA. *Mtb* stimulation increased the frequency of Thy1.1$^+$ cells in both *Bhlhe40*$^{+/+}$ and *Bhlhe40*$^{-/-}$ cultures

relative to unstimulated cultures, and this increase was greater in *Bhlhe40*$^{-/-}$ cells compared with *Bhlhe40*$^{+/+}$ cells (Fig. 5 D). *Mtb* stimulation also increased the amount of Thy1.1 expression on a per-cell basis, where *Bhlhe40*$^{-/-}$ CD11c$^+$CD11b$^+$MHC-II^{high} (GM-DC) cells exhibited a 1.7-fold higher MFI than *Bhlhe40*$^{+/+}$ GM-DCs (Fig. 5 E). ELISAs confirmed that 10BiT$^+$ *Bhlhe40*$^{-/-}$ cells secreted more IL-10 than 10BiT$^+$ *Bhlhe40*$^{+/+}$ cells after stimulation with heat-killed *Mtb* (Fig. 5 F). These experiments confirm that loss of Bhlhe40 in GM-CSF–cultured cells results in higher levels of IL-10 production.

Bhlhe40 binds directly to the *Il10* locus in T$_H$1 cells and myeloid cells

We performed chromatin immunoprecipitation sequencing (ChIP-seq) experiments in in vitro–polarized T$_H$1 cells and GM-CSF–cultured bone marrow–derived cells to interrogate whether Bhlhe40 directly binds to the *Il10* locus in these cells as well as to identify other genes that may be directly regulated by Bhlhe40. We performed this research with *Bhlhe40*$^{+/+}$ and *Bhlhe40*$^{-/-}$ cells, where *Bhlhe40*$^{-/-}$ cells served as controls for nonspecific binding by the anti-Bhlhe40 antibody. Bhlhe40 bound 379 sites in *Bhlhe40*$^{+/+}$ GM-CSF–cultured cells and 5,532 sites in *Bhlhe40*$^{+/+}$ T$_H$1-polarized T cells (Tables S1 and S2). Of these sites, 273 were found in both datasets. Bhlhe40 can directly bind to regulatory DNA elements as a homodimer through recognition of E-box sites, with a preference for the sequence CACGTG (St-Pierre et al., 2002). Motif finding identified the expected E-box (CACGTG) as the most frequent motif present within the peaks identified in both cell types (Fig. 6 A). Analysis of binding sites revealed that Bhlhe40 predominantly bound promoters within 1 kb of the transcriptional start site, introns, and distal intergenic regions (Fig. 6 B). Pathway analysis of predicted Bhlhe40-regulated genes revealed an enrichment in immune activation and cytokine response pathways in both datasets (Fig. 6 C). Bhlhe40 is known to bind a conserved autoregulatory site in the *Bhlhe40* promoter (Sun and Taneja, 2000), and this binding site was identified as a peak in both datasets (Fig. 6 D). Importantly, our ChIP-seq experiment identified a Bhlhe40 binding site at +6 kb relative to the transcriptional start site of *Il10* in both datasets, coinciding with an evolutionarily conserved region that is close to a +6.45-kb site previously identified as an enhancer element in T$_H$2 cells (Fig. 6 D; Jones and Flavell, 2005). These data suggest that Bhlhe40 directly represses *Il10* transcription in myeloid and lymphoid cells through direct binding of a downstream cis-regulatory element. ChIP-seq analysis did not reveal binding of Bhlhe40 to the *Il12b* locus in either dataset (Tables S1 and S2). Bhlhe40 did not bind the *Ifng* locus in GM-CSF–cultured cells but bound two sites distal (−33.5 kb and +53.2 kb) to the *Ifng* transcriptional start site in T$_H$1 cells (Fig. S5 B). These findings suggest that the transcriptional down-regulation of *Il12b* in *Bhlhe40*$^{-/-}$ total lung samples (Fig. 4 D) is indirect and likely a result of increased IL-10 signaling, whereas the decreased levels of *Ifng* may result from either increased IL-10 signaling or T cell–intrinsic loss of direct regulation by Bhlhe40.

IL-10 deficiency protects *Bhlhe40*$^{-/-}$ mice from *Mtb* infection

To investigate the role of IL-10 production in the susceptibility of *Bhlhe40*$^{-/-}$ mice, we generated *Il10*$^{-/-}$*Bhlhe40*$^{-/-}$ mice and
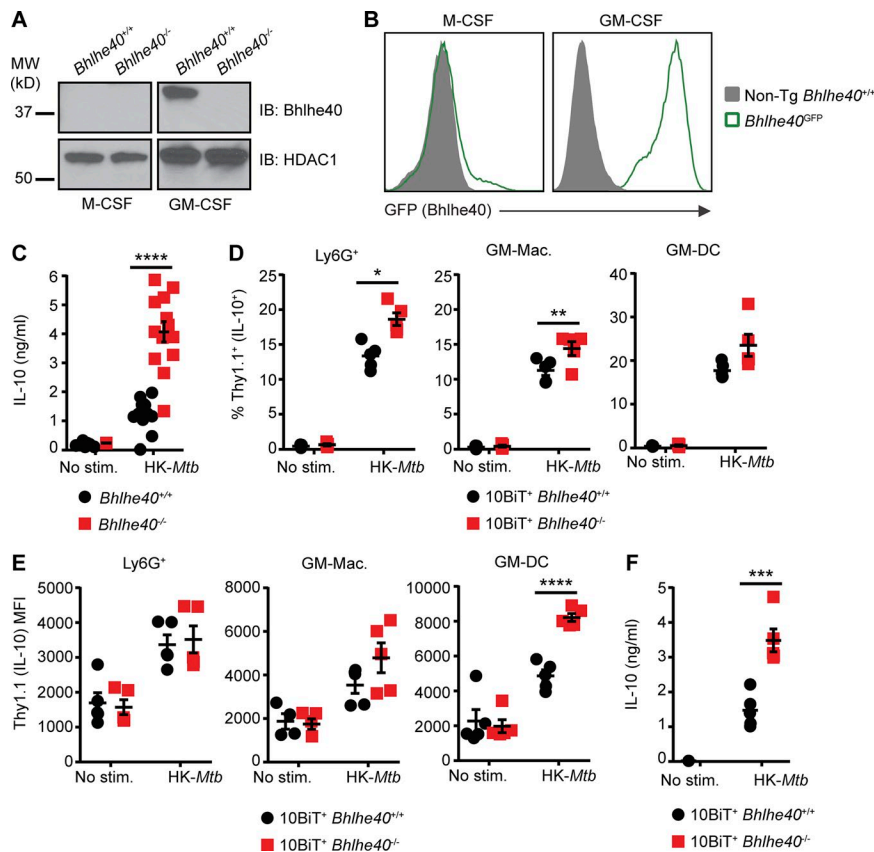
Figure 5. **Bhlhe40 represses IL-10 in myeloid cells after *Mtb* stimulation. (A and B)** *Bhlhe40+/+*, *Bhlhe40−/−*, and *Bhlhe40GFP* bone marrow cells were differentiated in the presence of M-CSF or GM-CSF and analyzed for expression of Bhlhe40 by immunoblot (IB) with HDAC1 as a loading control (A) or GFP as a reporter for Bhlhe40 expression (B). MW, molecular weight. **(C)** *Bhlhe40+/+* and *Bhlhe40−/−* GM-CSF–cultured bone marrow–derived cells were left unstimulated or stimulated with heat-killed (HK) *Mtb* (n = 13 per group) for 24 h, and culture supernatants were analyzed for IL-10 production by ELISA. IL-10 expression in six unstimulated *Bhlhe40+/+* and 12 unstimulated *Bhlhe40−/−* samples was below the limit of detection (∼0.1 ng/ml). **(D–F)** 10BiT+ *Bhlhe40+/+* and *Bhlhe40−/−* bone marrow cells were differentiated in the presence of GM-CSF and stimulated with heat-killed *Mtb* antigen for 24 h. Thy1.1 was assessed on three subpopulations of cells within the GM-CSF cultures. These included Ly6G+ cells, GM-macrophages (GM-Macs; identified as CD11c+CDllbhiMHC-IImid), and GM-DCs (identified as CD11c+CD11bmidMHC-IIhi). **(D)** Frequency of Thy1.1+ (IL-10+) cells after 24 h of stimulation (n = 5 per group). **(E)** Geometric MFI for Thy1.1 on Thy1.1+ cells after 24 h of stimulation (n = 5 per group). **(F)** Culture supernatants were analyzed for IL-10 production by ELISA (n = 5 per group). IL-10 expression in four unstimulated 10BiT+ *Bhlhe40+/+* and five unstimulated 10BiT+ *Bhlhe40−/−* samples was below the limit of detection (∼0.1 ng/ml). Each point represents data from cells derived from a single mouse. The mean ± SEM is graphed. Statistical differences were determined by two-tailed unpaired Student's *t* test for normally distributed groups or two-tailed unpaired Mann-Whitney test for nonnormally distributed groups. *, P < 0.05; **, P < 0.01; ***, P < 0.001; ****, P < 0.0001. Data are from or representative of two (A, B, and D–F) or five (C) independent experiments.

compared their survival to *Bhlhe40+/+*, *Bhlhe40−/−*, and *Il10−/−* mice after *Mtb* infection. The absence of IL-10 signaling resulted in near-complete rescue of the susceptibility phenotype caused by Bhlhe40 deficiency as shown by the significant increase in the median survival time of *Il10−/−Bhlhe40−/−* mice (>100 d) compared with *Bhlhe40−/−* mice (31 d; Fig. 7 A). The increased survival of *Il10−/−Bhlhe40−/−* mice was accompanied by an eightfold decrease in pulmonary *Mtb* titer in *Il10−/−Bhlhe40−/−* lungs compared with *Bhlhe40−/−* lungs at 21 dpi (Fig. 7 B). These data demonstrate that the inability of *Bhlhe40−/−* mice to control *Mtb* replication is likely caused in large part by higher IL-10 levels. When compared with *Bhlhe40−/−* lungs, *Il10−/−Bhlhe40−/−* lungs contained a significantly lower frequency and total number of neutrophils (Fig. 7, C and D). However, the frequency of neutrophils in *Il10−/−Bhlhe40−/−* lungs remained higher than in *Bhlhe40+/+* or *Il10−/−* lungs (Fig. 7, C and D). *Il10−/−Bhlhe40−/−* lungs also contained twofold more *Il12b* and *Ifng* transcripts than *Bhlhe40−/−* lungs at 21 dpi, demonstrating that IL-10 signaling was at least partially responsible for the decreased expression of these genes in *Bhlhe40−/−* lungs (Fig. 7 E). These data establish Bhlhe40 as an essential regulator of *Il10* expression in myeloid cells and lymphocytes during *Mtb* infection and reveal the importance of IL-10 regulation for innate and adaptive immune responses that control *Mtb* infection.

Discussion

We have identified Bhlhe40 as a transcription factor that is essential for coordinating immune responses that protect the host from *Mtb* infection. Based on our research, we propose the following model (Fig. 8). During the acute phase of infection, CD11c+ cells encounter *Mtb* antigens that trigger a putative transcriptional activator to induce *Il10* expression, the activity of which is restricted by the binding of Bhlhe40 to a cis-acting regulatory region +6 kb downstream of the *Il10* transcriptional start site. The identity of the activator that induces *Il10* transcription in the absence of Bhlhe40 during *Mtb* infection is currently unknown, but may be one of the activators previously described (Gabryšová et al., 2014). In addition, Bhlhe40 is induced in T cells during *Mtb* infection, where it also represses *Il10* transcription. The repression of *Il10* expression by Bhlhe40 in these cell types allows for higher expression of *Il12b* and *Ifng*, both of which are essential for control of *Mtb* replication (Cooper et al., 1993; Flynn et al., 1993; Hölscher et al., 2001). These findings represent the first study of roles for Bhlhe40 in the immune response to an infection and within myeloid cells. Additionally, although other negative regulators of *Il10* transcription have been described (Riemann et al., 2005; Yee et al., 2005; Villagra et al., 2009; Kang et al., 2010; Krausgruber et al., 2011), Bhlhe40 is the first transcription
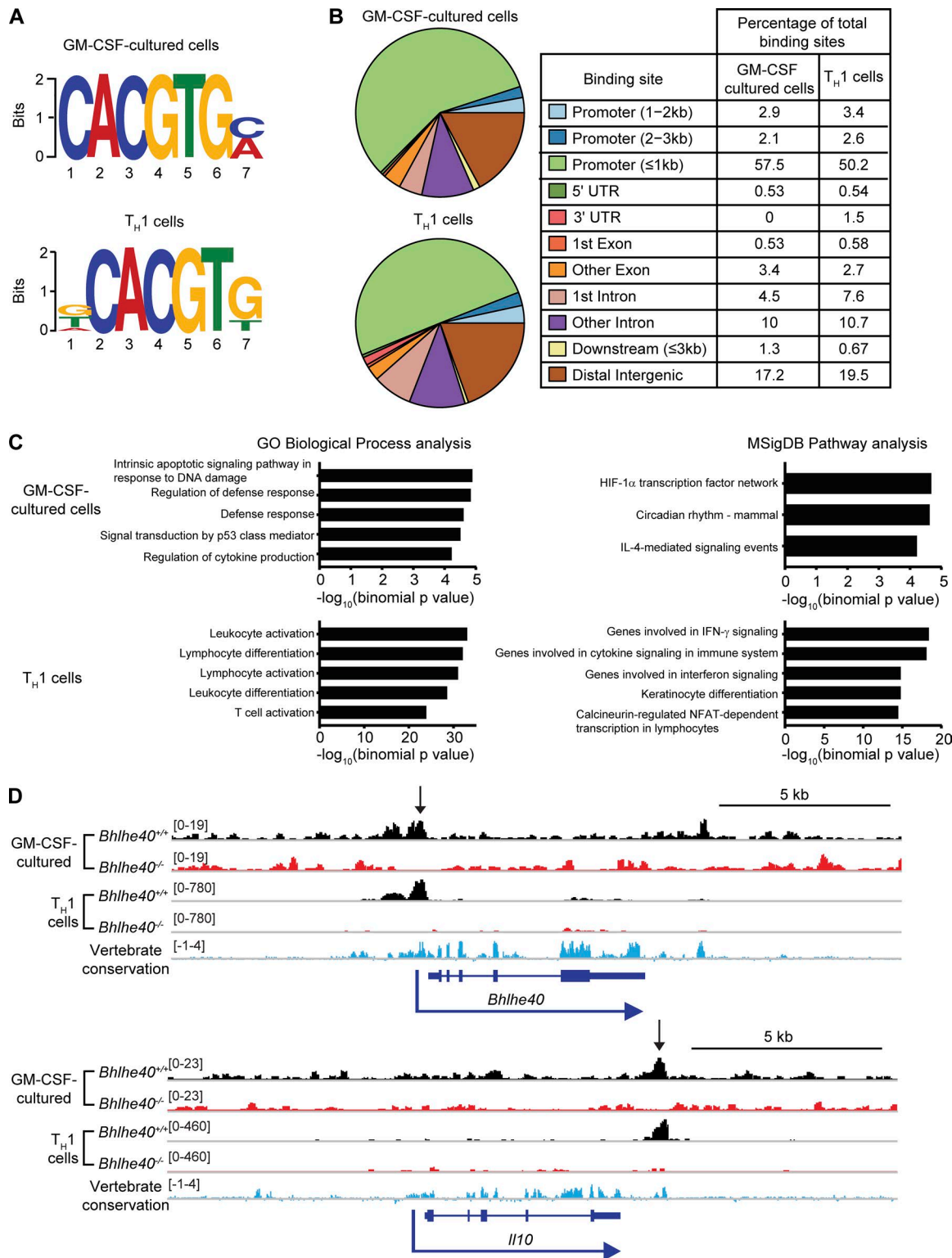
Figure 6. **Bhlhe40 directly binds the *Il10* locus in myeloid and lymphoid cells. (A–D)** Bone marrow cells were differentiated in the presence of GM-CSF and stimulated with heat-killed *Mtb* for 4 h. CD4+ T cells were T_H1 polarized in vitro for 4 d. DNA was immunoprecipitated using anti-Bhlhe40 antibody and sequenced. **(A)** Sequence motifs present within DNA bound by Bhlhe40 were analyzed by MEME-ChIP. **(B)** Bhlhe40 binding sites were annotated using ChIP-seeker (3.5). **(C)** Functions of cis-regulatory regions were predicted for Bhlhe40 binding site data using GREAT. The top five most highly enriched gene sets with minimum region-based fold enrichment of 2 and binomial and hypergeometric false discovery rates of ≤0.05 in the Gene Ontology (GO) Biological Process and MSigDB Pathway gene sets are displayed for each dataset (in GM-CSF–cultured cells, only three MSigDB Pathway gene sets met these criteria). NFAT, nuclear factor of activated T cells. **(D)** ChIP-seq binding tracks for Bhlhe40 at the *Bhlhe40* and *Il10* loci in *Bhlhe40+/+* and *Bhlhe40−/−* myeloid and lymphoid cells. Vertebrate conservation of each genomic region is displayed in blue, and peaks identified by MACS are indicated by arrows. Bracketed numbers indicate the trace height range. Data are from a single experiment.
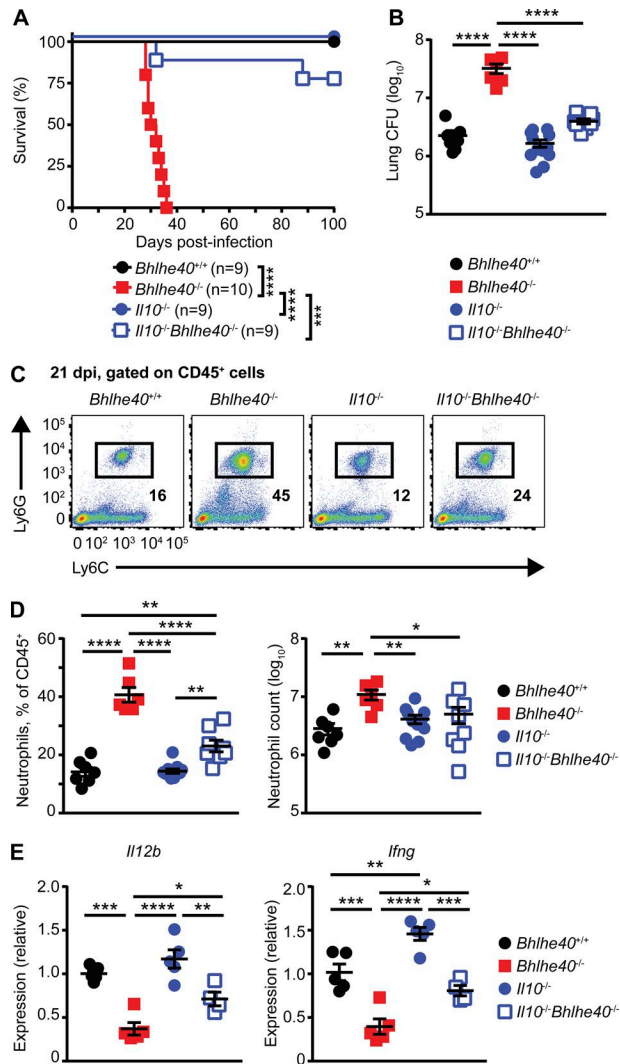
Figure 7. IL-10 deficiency protects *Bhlhe40*⁻/⁻ mice from *Mtb* infection. (A and B) *Bhlhe40*⁺/⁺, *Bhlhe40*⁻/⁻, *Il10*⁻/⁻, and *Il10*⁻/⁻*Bhlhe40*⁻/⁻ mice were monitored for survival after *Mtb* infection (A; *n* = 9–10 per group) or analyzed for pulmonary CFU at 21 dpi (B; *n* = 6–12 per group). The number of biological replicates is indicated in parentheses. (C) Representative flow cytometry plots for lung neutrophils as percentages of the total CD45⁺ population at 21 dpi. (D) The absolute neutrophil count and the frequency of neutrophils in the total lung CD45⁺ population 21 dpi (*n* = 6–12 per group). (E) Cytokine transcript levels in total lung samples at 21 dpi (*n* = 4–5 per group). Each point represents data from one mouse. The mean ± SEM is graphed. Statistical differences were determined by log-rank Mantel-Cox test (A) and one-way unpaired ANOVA with Tukey's post test for normally distributed groups or unpaired Kruskal-Wallis test with Dunn's multiple comparison test for nonnormally distributed groups (B, D, and E). *, P < 0.05; **, P < 0.01; ***, P < 0.001; ****, P < 0.0001. Data are from two (A and E) or four (B and D) independent experiments. Data in C are representative of four independent experiments.

factor that has been shown to be essential during *Mtb* infection specifically to regulate *Il10* expression. Our findings reveal the importance of controlling IL-10 generation by both innate and adaptive immune cells and shed light on how different levels of IL-10 could impact TB disease in humans.

Survival experiments showed that about one quarter of *Bhlhe40*ᶠˡ/ᶠˡ-*Cd11c-Cre* and *Bhlhe40*ᶠˡ/ᶠˡ-*Cd4-Cre* mice recapitulated the very early susceptibility of *Bhlhe40*⁻/⁻ mice (Fig. 3 D),
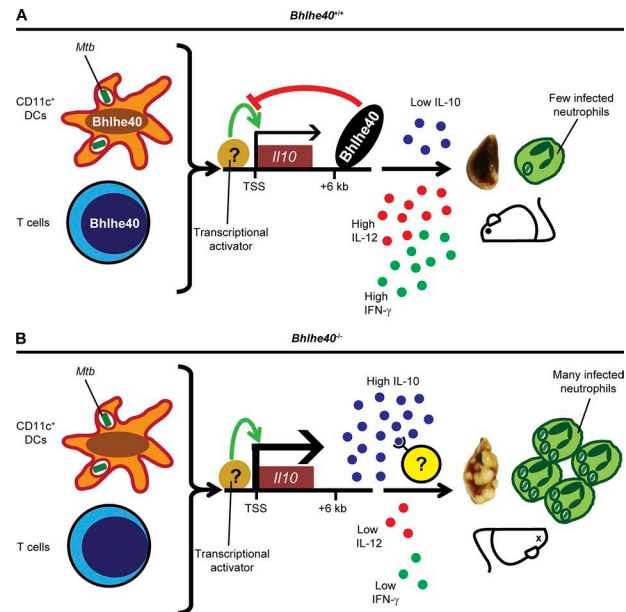

Figure 8. Model of Bhlhe40 function during *Mtb* infection. (A) During *Mtb* infection, *Il10* transcription is restricted by Bhlhe40 in CD11c⁺ DCs and T cells through direct binding to an enhancer site +6 kb downstream of the *Il10* transcriptional start site (TSS). The resulting amount of IL-10 expression is insufficient to compromise host resistance, leading to an immunological stalemate in which *Mtb* replication is controlled for the remainder of the lifetime of the host. **(B)** In *Bhlhe40*⁻/⁻ mice, the absence of Bhlhe40 in CD11c⁺ DCs and T cells allows for high levels of *Il10* expression. Excessive IL-10 signaling then acts on lung immune cells to suppress the production and protective effects of IL-12 and IFN-γ, both of which are essential for control of *Mtb* pathogenesis. As a result, in *Bhlhe40*⁻/⁻ mice, *Mtb* lung burdens are higher, and neutrophil-dominated inflammation is uncontrolled, ultimately resulting in susceptibility.

with the remainder of these Bhlhe40 conditionally deleted mice dying between 50 and 75 dpi. In the case of the *Bhlhe40*ᶠˡ/ᶠˡ-*Cd4-Cre* strain, the finding that 4 out of 12 of these mice succumbed at 31–38 dpi (Fig. 3 D), whereas *Rag1*⁻/⁻ mice succumbed at ∼45 dpi (Fig. 3 B), indicates that *Bhlhe40*⁻/⁻ T cells can be actively pathological and generate a worse outcome than the absence of T cells, likely through the production of a factor such as IL-10. The delay in susceptibility of most of the *Bhlhe40*ᶠˡ/ᶠˡ-*Cd11c-Cre* and *Bhlhe40*ᶠˡ/ᶠˡ-*Cd4-Cre* mice as compared with *Bhlhe40*⁻/⁻ mice could indicate that the susceptibility of *Bhlhe40*⁻/⁻ mice is a result of the combination of loss of Bhlhe40 in both CD11c⁺ and T cells, insufficient ability of the *Cd11c* and *Cd4* promoters to drive *Bhlhe40* exon deletion in all Cre-expressing cells, or the ability of Bhlhe40 deficiency in a non-CD11c⁺ or -CD4⁺ cell type to enhance susceptibility. IL-10 production by T cells and CD11c⁺ cells during *Mtb* infection in mice was recently shown to contribute to host susceptibility (Moreira-Teixeira et al., 2017), further supporting the notion that regulation of *Il10* expression in these cell populations would be important during *Mtb* infection.

Our analyses of *Il10*⁻/⁻*Bhlhe40*⁻/⁻ mice revealed that IL-10 deficiency conferred a near-complete rescue of multiple phenotypes associated with the susceptibility of *Bhlhe40*⁻/⁻ mice (Fig. 7), indicating that the up-regulation of *Il10* transcription in the absence of Bhlhe40 is a major contributor to the susceptibility of these mice. Nonetheless, some phenotypes partially

remained in the absence of *Il10*. For example, although the susceptibility of *Bhlhe40*^{+/+} and *Il10*^{−/−}*Bhlhe40*^{−/−} mice was not significantly different, we did observe that ∼20% of the *Il10*^{−/−} *Bhlhe40*^{−/−} mice succumbed before 100 dpi (Fig. 7 A). Additionally, *Il10*^{−/−}*Bhlhe40*^{−/−} mice had a significantly higher frequency of neutrophils in the lungs at 21 dpi compared with *Bhlhe40*^{+/+} mice (Fig. 7, C and D). The incomplete rescue of these phenotypes indicates that Bhlhe40 likely regulates the expression of other genes during *Mtb* infection that impact pathogenesis. Future studies will explore the other Bhlhe40-bound loci identified by ChIP-seq to identify additional Bhlhe40 targets that contribute to the control of *Mtb* infection.

Patients with active TB have increased levels of IL-10 in their serum (Verbon et al., 1999; Olobo et al., 2001) and lungs (Barnes et al., 1993; Huard et al., 2003; Bonecini-Almeida et al., 2004; Almeida et al., 2009), suggesting a link between increased IL-10 levels and TB disease (Redford et al., 2011). Although it is unclear whether the reduced expression of *BHLHE40* in the blood of patients with active TB (Fig. 1 A) is a cause or effect of their disease or related to the higher IL-10 levels found in this form of TB, this correlation agrees with the increased susceptibility of mice lacking *Bhlhe40* and suggests that our experiments could be relevant to human *Mtb* infection.

Materials and methods

Bacterial cultures
Mtb strain Erdman and its derivatives were cultured at 37°C in 7H9 broth (Sigma-Aldrich) or on 7H11 agar (BD) medium supplemented with 10% oleic acid/albumin/dextrose/catalase, 0.5% glycerol, and 0.05% Tween-80 (broth only). GFP-expressing *Mtb* (GFP-*Mtb*) was generated by transformation of *Mtb* strain Erdman with a plasmid (pMV261-kan-GFP) that drives constitutive expression of GFP under the control of the mycobacterial *hsp60* promoter. Cultures were grown in the presence of kanamycin to ensure plasmid retention.

L. monocytogenes expressing chicken ovalbumin (LM-Ova) on the 10403S genetic background was a gift from H. Shen (University of Pennsylvania, Philadelphia, PA). Bacteria were grown to mid-logarithmic phase with shaking at 37°C in brain–heart infusion broth (HiMedia Laboratories) before washing and storage as glycerol stocks at −80°C.

Mouse strains
All mice used were on a C57BL/6 background. C57BL/6 (Taconic), B6.SJL (CD45.1; Taconic), *Bhlhe40*[GFP] BAC Tg (N10 to C57BL/6; Lin et al., 2016), *Bhlhe40*^{−/−} (N10 to C57BL/6; Sun et al., 2001), *Rag1*^{−/−}, *Il10*^{−/−}, and 10BiT IL-10 reporter mice (Maynard et al., 2007) were maintained in a specific pathogen-free facility. *Bhlhe40*^{−/−} mice were crossed to *Rag1*^{−/−}, *Il10*^{−/−}, or 10BiT mice for some experiments.

Bhlhe40^{fl/fl} mice were generated with two loxP sites flanking exon 4 of *Bhlhe40*. These mice originated as a KO-first promoter-driven mouse line from the Knockout Mouse Project (KOMP) and were purchased from The Jackson Laboratory (*Bhlhe40*[tm1a(KOMP)Wtsi]; 024395). These initial mice contained a *Bhlhe40* allele with a splice acceptor–LacZ reporter and a

Neo cassette flanked by two Frt sites, which were removed by crossing them to B6N.129S4-*Gt(ROSA)26Sor*[tm1(FLP1)Dym]/J mice (016226; The Jackson Laboratory), leaving behind an allele of Bhlhe40 with a loxP-flanked exon 4. Subsequent crosses yielded *Bhlhe40*^{fl/fl} mice with no residual Rosa26-Flp transgene. *Bhlhe40*^{fl/fl} mice were crossed with one of four mouse strains, *Mrp8-Cre* (B6.Cg-Tg(S100A8-cre,-EGFP)1Ilw/J; 021614), *Lysm-Cre* (B6N.129P2(B6)-*Lyz2*[tm1(cre)Ifo]/J; 018956), *Cd11c-Cre* (B6. Cg-Tg(Itgax-cre)1-1Reiz/J; 008068), and *Cd4-Cre* (B6.Cg-Tg(Cd4-cre)1Cwi/Bflu/J; 022071), all from The Jackson Laboratory.

Age-matched littermate adult mice (9–23 wk of age) of both sexes were used, and mouse experiments were randomized. No blinding was performed during animal experiments. All procedures involving animals were conducted following the National Institutes of Health guidelines for housing and care of laboratory animals, and they were performed in accordance with institutional regulations after protocol review and approval by the Institutional Animal Care and Use Committee of The Washington University in St. Louis School of Medicine (protocol 20160094, Immune System Development and Function, and protocol 20160118, Analysis of Mycobacterial Pathogenesis). Washington University is registered as a research facility with the United States Department of Agriculture and is fully accredited by the American Association of Accreditation of Laboratory Animal Care. The Animal Welfare Assurance is on file with Office for Protection from Research Risks–National Institutes of Health. All animals used in these experiments were subjected to no or minimal discomfort. All mice were euthanized by CO_2 asphyxiation, which is approved by the American Veterinary Association Panel on Euthanasia.

Generation of bone marrow chimeric mice
Bone marrow chimeric mice were generated by lethal irradiation (1,000 rads) of *Bhlhe40*^{+/+} or *Bhlhe40*^{−/−} recipients and reconstitution with 1–2 × 10^{7} bone marrow cells from *Bhlhe40*^{+/+} or *Bhlhe40*^{−/−} donors. Mixed bone marrow chimeric mice were generated by lethal irradiation (1,000 rads) of *Bhlhe40*^{+/+} (CD45.1/.2) recipients and reconstitution with 1–2 × 10^{7} bone marrow cells from *Bhlhe40*^{+/+} (CD45.1/.1) and either *Bhlhe40*^{+/+} (CD45.2/.2) or *Bhlhe40*^{−/−} (CD45.2/.2) donors mixed at a 1:1 ratio before transfer. Mice received drinking water containing 1.3 mg sulfamethoxazole and 0.26 mg trimethoprim per ml for 2 wk after reconstitution and were allowed to reconstitute for at least 8 wk before infection with *Mtb*.

Cell culture
Bone marrow cells were isolated from femurs and tibias of mice and treated with ACK lysis buffer (0.15 M NH_4Cl, 10 mM $KHCO_3$, and 0.1 mM EDTA) to lyse red blood cells. To generate M-CSF bone marrow–derived macrophages, bone marrow cells were cultured in complete IMDM (10% heat-inactivated FBS + 2 mM ʟ-glutamine + 1× penicillin/streptomycin + 55 µM β-mercaptoethanol + 1× MEM nonessential amino acids + 1 mM sodium pyruvate) in Petri dishes with the addition of 20 ng/ml M-CSF (PeproTech). To generate GM-CSF–cultured bone marrow–derived DCs and macrophages, bone marrow cells were cultured in complete RPMI (10% heat-inactivated FBS + 2 mM ʟ-glutamine + 1× penicillin/

streptomycin + 55 µM β-mercaptoethanol) in six-well plates with the addition of 20 ng/ml GM-CSF (PeproTech). Cells were incubated at 37°C in 8% CO_2 for 8–9 d. At the end of the cultures, cells were harvested, counted, and adjusted to the desired cell concentrations. For flow cytometry analysis and ELISA assays, cells were seeded at a concentration of $5 × 10^5$ cells/well in 96-well plates and were stimulated with or without 50 µg/ml heat-killed *Mtb* (H37Ra strain; Difco) for 18 (FACS) or 24 (ELISA) h. In some experiments, suspension cells were stimulated in the presence of 10 µg/ml heat-killed *Mtb* (H37Ra strain; Difco) for 4 h for ChIP assays.

To generate in vitro–polarized T_H1 cells, naive splenic $CD4^+$ T cells (Easysep mouse naive $CD4^+$ T cell isolation kit, typical purity ~90–96%; StemCell Technologies, Inc.) were cultured in IMDM with plate-bound anti-CD3 (2 µg/ml; clone 145-2C11; BioLegend) and anti-CD28 antibodies (2 µg/ml; clone 37.51; BioLegend) in the presence of IL-12 (10 ng/ml; BioLegend) and anti-IL-4 (20 µg/ml; Leinco). Cultures were split on day 3 and used for ChIP-seq on day 4.

For *Mtb* infection, cells were seeded at a concentration of $2.5 × 10^5$ cells/well in 96-well plates. *Mtb* was washed with PBS + 0.05% Tween-80, sonicated to disperse clumps, diluted in antibiotic-free cell culture media, and added to cells at a multiplicity of infection of 1. After 4 h of incubation, cells were pelleted and washed twice with PBS, fresh culture media was added, and cells were incubated at 37°C in 5% CO_2. In some cases, cells were pretreated with 250 U IFN-γ (BioLegend) for 12 h before infection. CFUs were enumerated by pelleting cells, removing supernatant, lysing with PBS + 0.5% Triton X-100, and plating serial dilutions on 7H11 agar. Colonies were counted after 3 wk of incubation at 37°C in 5% CO_2.

Mtb infection of mice
Mtb cultures in logarithmic growth phase (OD_{600} = 0.5–0.8) were washed with PBS + 0.05% Tween-80, sonicated to disperse clumps, and diluted in sterile water. Mice were exposed to $1.6 × 10^8$ *Mtb* CFUs, a dose chosen to deliver 100–200 CFUs of aerosolized *Mtb* per lung using an Inhalation Exposure System (Glas-Col). Within the first 24 h of each infection, lungs were harvested from at least two control mice, homogenized, and plated on 7H11 agar to determine the input CFU dose. The mean dose determined at this time point was assumed to be representative of the dose received by all other mice infected simultaneously. At each time point after infection, *Mtb* titers were determined by homogenizing the superior, middle, and inferior lobes of the lung or the entire spleen and plating serial dilutions on 7H11 agar. Colonies were counted after 3 wk of incubation at 37°C in 5% CO_2.

L. monocytogenes infection of mice
LM-Ova was diluted into pyrogen-free saline for i.v. injection into mice. For experiments involving secondary infection, some mice were initially infected with a sublethal dose of 10^4 LM-Ova i.v. and rested for 30 d before secondary challenge with 10^6 LM-Ova i.v. After 3 d, spleens and livers were homogenized separately in PBS + 0.05% Triton X-100. Homogenates were plated on brain–heart infusion agar, and *L. monocytogenes* CFUs were determined after growth at 37°C overnight.

Flow cytometry
Lungs were perfused with sterile PBS before harvest. Lungs and lymph nodes were digested at 37°C with 630 µg/ml collagenase D (Roche) and 75 U/ml DNase I (Sigma-Aldrich). All antibodies were used at a dilution of 1:200. Single-cell suspensions were preincubated with anti-CD16/CD32 Fc Block antibody (BD) in PBS + 2% heat-inactivated FBS for 10 min at RT before surface staining. The following anti–mouse antibodies were obtained from BioLegend: PE-Cy7 anti-CD4 (RM4-5), APC-Cy7 anti-CD8α (53–6.7), APC anti-CD11b (M1/70), BV605 anti-CD11c (N418), BV605 anti-CD19 (6D5), APC anti-CD45.2 (104), FITC anti-CD90.1 (Thy-1.1; OX-7), PerCP-Cy5.5 anti-CD103 (2E7), Pacific blue (PB) or PerCP-Cy5.5 anti-Ly6C (HK1.4), PE anti-Ly6G (1A8), PB anti-TCRβ (H57-597), and APC anti-TCR γδ (GL3). The following anti–mouse antibodies were purchased from BD: PB anti-CD3ε (145-2C11), BV510 anti-CD45 (30F11), and PE anti–Siglec F (E50-2440). The following anti–mouse antibodies were obtained from Tonbo Biosciences: redFluor710 anti-CD44 (IM7), V450 or PerCP-Cy5.5 anti-CD45.1 (A20), PE-Cy7 anti-Ly6G (1A8), and redFluor710 anti-I-A/I-E (M5/114.15.2).

Cells were stained for 20 min at 4°C, washed, and fixed in 4% paraformaldehyde (Electron Microscopy Sciences) in PBS for 20 min at 4°C. Cell counts were determined by hemocytometer.

For identification of antigen-specific T cells, APC-conjugated tetramers of $Ag85B_{280–294}$ peptide (FQDAYNAAGGHNAVF) or $ESAT6_{4–17}$ peptide (QQWNFAGIEAAASA) bound to MHC-II$^{I-A(b)}$ (National Institutes of Health Tetramer Core) were added to digested cells at final dilutions of 1:25 or 1:100, depending on the age of the tetramer stock, and incubated at RT for 75 min. Cells were then surface stained as above. Antigen-specific cells were defined as $CD45^+$/$CD3ε^+$/$CD4^+$/$CD44^+$/tetramer$^+$.

Flow cytometry data were acquired on an LSR Fortessa cytometer (BD) and analyzed using FlowJo software (TreeStar). Gating strategies are depicted in Fig. S5 (C and D). Gates for Tg (*Bhlhe40*^{GFP} and 10BiT) mice were set using nontransgenic mice to control for background staining.

Neutrophil depletion
Mice were intraperitoneally injected with 200 µg monoclonal anti-Ly6G antibody (clone 1A8; BioXCell or Leinco) or 200 µg polyclonal rat serum IgG (Sigma-Aldrich) diluted in sterile PBS (HyClone) every 48 h beginning at 10 dpi and ending at 30 dpi.

Quantitative RT-PCR
Lung samples were lysed by bead-beating in TRIzol reagent (Invitrogen), pelleted to remove beads, and stored at –80°C until RNA extraction. RNA was purified from TRIzol using the Direct-zol RNA miniprep kit (Zymo Research) and immediately reverse transcribed with SuperScript III reverse transcription using OligodT primers (Thermo Fisher Scientific). Quantitative RT-PCR was performed using iTAQ SYBR green (Bio-Rad Laboratories) on a C1000 thermal cycler with the CFX96 real-time system (Bio-Rad Laboratories). Transcript levels were analyzed using the $2^{ΔΔCt}$ method normalized to *Actb* (β-actin) as the reference gene. The following primers were used: *Actb* forward, 5′-ACCTTCTACAAT GAGCTGCG-3′; *Actb* reverse, 5′-CTGGATGGCTACGTACATGG-3′; *Ccl3* forward, 5′-ACACTCTGCAACCAAGTCTTC-3′; *Ccl3* reverse,

Huynh et al.
Bhlhe40 represses IL-10 during *M. tuberculosis* infection

Journal of Experimental Medicine
https://doi.org/10.1084/jem.20171704

1834

5′-AGGAAAATGACACCTGGCTG-3′; *Ccl4* forward, 5′-CTGTTT CTCTTACACCTCCCG-3′; *Ccl4* reverse, 5′-TGTCTGCCTCTTTTG GTCAG-3′; *Ifng* forward, 5′-CCTAGCTCTGAGACAATGAACG-3′; *Ifng* reverse, 5′-TTCCACATCTATGCCACTTGAG-3′; *Il10* forward, 5′-AGCCTTATCGGAAATGATCCAGT-3′; *Il10* reverse, 5′-GGCCTT GTAGACACCTTGGT-3′; *Il12b* forward 5′-ACTCCCCATTCCTAC TTCTCC-3′; and *Il12b* reverse, 5′-CATTCCCGCCTTTGCATTG-3′.

Western blots

Bone marrow–derived cells were counted and lysed at $10^6/40$ µl in Laemmli sample buffer (Bio-Rad Laboratories) containing 2.5% β-mercaptoethanol. Cell lysates were loaded and separated by 12% SDS-PAGE (Bio-Rad Laboratories) and transferred to Bio-Blot–polyvinylidene difluoride membranes (Costar). Blots were incubated with anti-Bhlhe40 (1:1,000; NB100-1800, Lot A; Novus Biologicals) or anti-HDAC1 (1:2,000; Abcam) primary antibodies at 4°C overnight with shaking. Blots were washed four to five times before incubation with anti–rabbit IgG-HRP (clone 5A6-1D10 [light chain specific]; Jackson ImmunoResearch Laboratories, Inc.) at RT for 60 min with shaking. After five washes, Clarity Western ECL substrate (Bio-Rad Laboratories) was applied, and blots were placed on blue basic autoradiography film (Gene-Mate). Film was developed with a medical film processor (model SRX-101A; Konica Minolta).

Cytokine ELISAs

IL-10 ELISA assays were performed on Nunc Maxisorp plates using IL-10 ELISPOT antibody pairs (BD). The enzyme reaction was developed with streptavidin-HRP (BioLegend) and 3,3′,5,5′-tetramethylbenzidine substrate (BioLegend). Recombinant mouse IL-10 (BioLegend) was used to generate the standard curve.

Histology

Lung samples were fixed in 10% buffered formalin (Thermo Fisher Scientific), embedded in paraffin, sectioned, and stained with H&E or Ziehl-Neelsen stain to identify acid-fast bacilli.

ChIP-seq

Anti-Bhlhe40 ChIP was modified from the protocol published by Chou et al. (2016). GM-CSF–cultured cells were harvested after 9 d and stimulated with 10 µg/ml heat-killed *Mtb* (strain H37Ra; Difco) for 4 h. In vitro–polarized T_H1 cells were stimulated with PMA (50 ng/ml; Enzo Life Sciences) and ionomycin (1 µM; Enzo Life Sciences) for 1.5 h. Stimulated cells were fixed for 10 min at RT with 1% paraformaldehyde with shaking. Cross-linked chromatin was fragmented by sonication and then immunoprecipitated with polyclonal rabbit anti-Bhlhe40 antibody (NB100-1800, Lot A or Lot C1; Novus Biologicals). After immunoprecipitation, DNA was purified by the GenElute PCR cleanup kit (Sigma-Aldrich).

Purified DNA was used for library construction followed by single-read sequencing on a HiSeq3000 system (Illumina) at the Genome Technology Access Center at Washington University in St. Louis. Read lengths were 101 bp and 50 bp in the case of GM-CSF–cultured bone marrow cells and T_H1 cells, respectively. Fastq files were provided by the Genome Technology Access Center sequencing facility. Quality control of fastq files was

performed using FastQC (0.11.3). Raw reads were mapped on the mm10 mouse reference genome using Bowtie (1.1.1). *Bhlhe40*$^{−/−}$ samples were used as input samples for peak calling on *Bhlhe40*$^{+/+}$ samples. Peak calling was performed using MACS v1.4 (Zhang et al., 2008) with the following flags: macs14-t WT-cKO-f BAM-g mm-n WTvsKO-p 0.00001.

BEDtools (2.6; bedClip and bedGraphToBigWig) were used to visualize raw alignments. Normalized tracks were built using Deeptools (2.5.3). The UCSC Genome Browser was used for visualization. R package ChIPseeker (1.14.1) was used for peak annotation. Multiple EM for Motif Elicitation (MEME)-ChIP (4.12.0; Machanick and Bailey, 2011) was used for motif enrichment analysis using all acquired peaks. Genomic Regions Enrichment of Annotations Tool (GREAT; 3.0.0) was used to predict the function of cis-regulatory regions for Gene Ontology Biological Process and MSigDB Pathway gene sets (McLean et al., 2010).

Links for raw sequencing data are available at GSE113054. All primary processed data (including mapped reads) for ChIP-seq experiments are also available there.

Analysis of human expression microarrays

We used the GEO2R web tool (www.ncbi.nlm.nih.gov/geo/geo2r) to query the expression of genes in three publically available GEO datasets (GSE19491 [Berry et al., 2010], GSE28623 [Maertzdorf et al., 2011], and GSE42834 [Bloom et al., 2013]) that compared the whole-blood transcriptomes of humans with active TB to other humans with either no disease, latent TB, or in some cases, lung cancer, pneumonia, or sarcoidosis. The following probesets were used to examine the expression of *BHLHE40* (previously called *BHLHB2*): for GSE19491 and GSE42834, ILMN_1768534; and for GSE28623, Agilent Technologies feature number 37383. The following probesets were used to examine the expression of *STAT1*: for GSE19491 and GSE42834, ILMN_1690105, ILMN_1691364, and ILMN_1777325; and for GSE28623, Agilent Technologies feature numbers 1928, 4610, 4763, 15819, 24587, 29771, 37967, and 42344. For analysis of GSE19491, the training and test sets, both encompassing samples from the United Kingdom, were combined, and the validation set containing samples from South Africa was analyzed separately. GSE28623 contained samples from The Gambia. For analysis of GSE42834, the training, test, and validation sets encompassing samples from the United Kingdom and France were combined.

Data and statistics

All data are from at least two independent experiments unless otherwise indicated. Samples represent biological (not technical) replicates of mice randomly sorted into each experimental group. No blinding was performed during animal experiments. Mice were excluded only when pathology unrelated to *Mtb* infection was present (i.e., weight loss caused by malocclusion or cage flooding). Statistical differences were calculated using Prism (7.0; GraphPad Software) using log-rank Mantel-Cox tests (survival), unpaired two-tailed Student's *t* tests (to compare two groups with normal distributions), unpaired two-tailed Mann-Whitney tests (to compare two groups with nonnormal distributions), one-way ANOVA with Tukey's multiple comparisons tests (to compare more than two groups with normal distributions), or unpaired

Huynh et al.
Bhlhe40 represses IL-10 during *M. tuberculosis* infection

Journal of Experimental Medicine
https://doi.org/10.1084/jem.20171704

1835

Kruskal-Wallis tests with Dunn's multiple comparisons tests (to compare more than two groups with nonnormal distributions). Normality was determined using a D'Agostino-Pearson omnibus normality test. Sample sizes were sufficient to detect differences as small as 10% using the statistical methods described. When used, center values and error bars represent means ± SEM.

Online supplemental material

Fig. S1 provides additional data on pulmonary histology, hematopoietic cell population numbers, *Mtb*-specific T cell frequencies, the number and MFI of *Mtb*+ lung cells, and analysis of neutrophil-depleted mice. Fig. S2 contains in vivo expression patterns of Bhlhe40 before and after *Mtb* infection. Fig. S3 provides additional analysis of *Mtb*-infected *Rag1*−/−*Bhlhe40*−/−, *Bhlhe40*fl/fl *Lysm-Cre*, *Bhlhe40*fl/fl *Mrp8-Cre*, and mixed bone marrow chimeric mice. Fig. S4 shows representative flow cytometry plots and absolute cell counts for lung immune cells from 10BiT IL-10 reporter mice. Fig. S5 shows that *Bhlhe40*−/− GM-CSF–cultured cells are not defective in control of *Mtb* infection, putative Bhlhe40 binding sites in the *Ifng* locus, and the flow cytometry gating strategies used throughout this study. Data on Bhlhe40 binding sites identified by ChIP-seq, predicted functions of associated cis-regulatory regions, and associated gene ontogeny analysis in GM-CSF–cultured cells and T_H1-polarized T cells are available in Tables S1 and S2, respectively.

Acknowledgments

Author contributions: J.P. Huynh, C.-C. Lin, B.T. Edelson, and C.L. Stallings designed the experiments, analyzed data, and wrote the manuscript. J.P. Huynh and J.M. Kimmey performed *Mtb* infections. J.P. Huynh and C.-C. Lin performed flow cytometry. E.A. Schwarzkopf and T.R. Bradstreet performed *L. monocytogenes* infections. C.-C. Lin, E.A. Schwarzkopf, T.R. Bradstreet, and N.N. Jarjour generated bone marrow chimeras. E.A. Schwarzkopf performed ELISA. N.N. Jarjour performed Western blots. C.-C. Lin and T.R. Bradstreet performed ChIP experiments. I. Shchukina, O. Shpynov, and M.N. Artyomov analyzed ChIP-seq data. C.T. Weaver and R. Taneja provided key mouse strains.

References

Abram, C.L., G.L. Roberge, Y. Hu, and C.A. Lowell. 2014. Comparative analysis of the efficiency and specificity of myeloid-Cre deleting strains using ROSA-EYFP reporter mice. *J. Immunol. Methods.* 408:89–100. https://doi.org/10.1016/j.jim.2014.05.009

Almeida, A.S., P.M. Lago, N. Boechat, R.C. Huard, L.C.O. Lazzarini, A.R. Santos, M. Nociari, H. Zhu, B.M. Perez-Sweeney, H. Bang, et al. 2009. Tuberculosis is associated with a down-modulatory lung immune response that impairs T_h1-type immunity. *J. Immunol.* 183:718–731. https://doi.org/10.4049/jimmunol.0801212

Barber, D.L., K.D. Mayer-Barber, C.G. Feng, A.H. Sharpe, and A. Sher. 2011. CD4 T cells promote rather than control tuberculosis in the absence of PD-1-mediated inhibition. *J. Immunol.* 186:1598–1607. https://doi.org/10.4049/jimmunol.1003304

Barnes, P.F., S. Lu, J.S. Abrams, E. Wang, M. Yamamura, and R.L. Modlin. 1993. Cytokine production at the site of disease in human tuberculosis. *Infect. Immun.* 61:3482–3489.

Beamer, G.L., D.K. Flaherty, B.D. Assogba, P. Stromberg, M. Gonzalez-Juarrero, R. de Waal Malefyt, B. Vesosky, and J. Turner. 2008. Interleukin-10 promotes *Mycobacterium tuberculosis* disease progression in CBA/J mice. *J. Immunol.* 181:5545–5550. https://doi.org/10.4049/jimmunol.181.8.5545

Berry, M.P.R., C.M. Graham, F.W. McNab, Z. Xu, S.A.A. Bloch, T. Oni, K.A. Wilkinson, R. Banchereau, J. Skinner, R.J. Wilkinson, et al. 2010. An interferon-inducible neutrophil-driven blood transcriptional signature in human tuberculosis. *Nature.* 466:973–977. https://doi.org/10.1038/nature09247

Bloom, C.I., C.M. Graham, M.P.R. Berry, F. Rozakeas, P.S. Redford, Y. Wang, Z. Xu, K.A. Wilkinson, R.J. Wilkinson, Y. Kendrick, et al. 2013. Transcriptional blood signatures distinguish pulmonary tuberculosis, pulmonary sarcoidosis, pneumonias and lung cancers. *PLoS One.* 8:e70630. https://doi.org/10.1371/journal.pone.0070630

Bonecini-Almeida, M.G., J.L. Ho, N. Boéchat, R.C. Huard, S. Chitale, H. Doo, J. Geng, L. Rego, L.C.O. Lazzarini, A.L. Kritski, et al. 2004. Down-modulation of lung immune responses by interleukin-10 and transforming growth factor β (TGF-β) and analysis of TGF-β receptors I and II in active tuberculosis. *Infect. Immun.* 72:2628–2634. https://doi.org/10.1128/IAI.72.5.2628-2634.2004

Bustamante, J., S. Boisson-Dupuis, L. Abel, and J.L. Casanova. 2014. Mendelian susceptibility to mycobacterial disease: genetic, immunological, and clinical features of inborn errors of IFN-γ immunity. *Semin. Immunol.* 26:454–470. https://doi.org/10.1016/j.smim.2014.09.008

Chou, C., D.J. Verbaro, E. Tonc, M. Holmgren, M. Cella, M. Colonna, D. Bhattacharya, and T. Egawa. 2016. The Transcription Factor AP4 Mediates Resolution of Chronic Viral Infection through Amplification of Germinal Center B Cell Responses. *Immunity.* 45:570–582. https://doi.org/10.1016/j.immuni.2016.07.023

Cooper, A.M., D.K. Dalton, T.A. Stewart, J.P. Griffin, D.G. Russell, and I.M. Orme. 1993. Disseminated tuberculosis in interferon gamma gene-disrupted mice. *J. Exp. Med.* 178:2243–2247. https://doi.org/10.1084/jem.178.6.2243

Demangel, C., P. Bertolino, and W.J. Britton. 2002. Autocrine IL-10 impairs dendritic cell (DC)-derived immune responses to mycobacterial

Huynh et al.
Bhlhe40 represses IL-10 during *M. tuberculosis* infection

Journal of Experimental Medicine
https://doi.org/10.1084/jem.20171704

1836

infection by suppressing DC trafficking to draining lymph nodes and local IL-12 production. *Eur. J. Immunol.* 32:994–1002. https://doi.org/10.1002/1521-4141(200204)32:4%3C994::AID-IMMU994%3E3.0.CO;2-6

de Waal Malefyt, R., J. Abrams, B. Bennett, C.G. Figdor, and J.E. de Vries. 1991. Interleukin 10(IL-10) inhibits cytokine synthesis by human monocytes: an autoregulatory role of IL-10 produced by monocytes. *J. Exp. Med.* 174:1209–1220. https://doi.org/10.1084/jem.174.5.1209

Feng, C.G., M.C. Kullberg, D. Jankovic, A.W. Cheever, P. Caspar, R.L. Coffman, and A. Sher. 2002. Transgenic mice expressing human interleukin-10 in the antigen-presenting cell compartment show increased susceptibility to infection with *Mycobacterium avium* associated with decreased macrophage effector function and apoptosis. *Infect. Immun.* 70:6672–6679. https://doi.org/10.1128/IAI.70.12.6672-6679.2002

Flynn, J.L., J. Chan, K.J. Triebold, D.K. Dalton, T.A. Stewart, and B.R. Bloom. 1993. An essential role for interferon gamma in resistance to *Mycobacterium tuberculosis* infection. *J. Exp. Med.* 178:2249–2254. https://doi.org/10.1084/jem.178.6.2249

Gabryšová, L., A. Howes, M. Saraiva, and A. O'Garra. 2014. The regulation of IL-10 expression. *Curr. Top. Microbiol. Immunol.* 380:157–190.

Gazzinelli, R.T., I.P. Oswald, S.L. James, and A. Sher. 1992. IL-10 inhibits parasite killing and nitrogen oxide production by IFN-gamma-activated macrophages. *J. Immunol.* 148:1792–1796.

Helft, J., J. Böttcher, P. Chakravarty, S. Zelenay, J. Huotari, B.U. Schraml, D. Goubau, and C. Reis e Sousa. 2015. GM-CSF Mouse Bone Marrow Cultures Comprise a Heterogeneous Population of CD11c(+)MHCII(+) Macrophages and Dendritic Cells. *Immunity.* 42:1197–1211. https://doi.org/10.1016/j.immuni.2015.05.018

Heng, T.S.P., and M.W. Painter. Immunological Genome Project Consortium. 2008. The Immunological Genome Project: networks of gene expression in immune cells. *Nat. Immunol.* 9:1091–1094. https://doi.org/10.1038/ni1008-1091

Hölscher, C., R.A. Atkinson, B. Arendse, N. Brown, E. Myburgh, G. Alber, and F. Brombacher. 2001. A protective and agonistic function of IL-12p40 in mycobacterial infection. *J. Immunol.* 167:6957–6966. https://doi.org/10.4049/jimmunol.167.12.6957

Hörber, S., D.G. Hildebrand, W.S. Lieb, S. Lorscheid, S. Hailfinger, K. Schulze-Osthoff, and F. Essmann. 2016. The atypical inhibitor of NF-κB, IκBζ, controls macrophage interleukin-10 expression. *J. Biol. Chem.* 291:12851–12861. https://doi.org/10.1074/jbc.M116.718825

Huard, R.C., S. Chitale, M. Leung, L.C.O. Lazzarini, H. Zhu, E. Shashkina, S. Laal, M.B. Conde, A.L. Kritski, J.T. Belisle, et al. 2003. The *Mycobacterium tuberculosis* complex-restricted gene *cfp32* encodes an expressed protein that is detectable in tuberculosis patients and is positively correlated with pulmonary interleukin-10. *Infect. Immun.* 71:6871–6883. https://doi.org/10.1128/IAI.71.12.6871-6883.2003

Iyer, S.S., and G. Cheng. 2012. Role of interleukin 10 transcriptional regulation in inflammation and autoimmune disease. *Crit. Rev. Immunol.* 32:23–63. https://doi.org/10.1615/CritRevImmunol.v32.i1.30

Jones, E.A., and R.A. Flavell. 2005. Distal enhancer elements transcribe intergenic RNA in the IL-10 family gene cluster. *J. Immunol.* 175:7437–7446. https://doi.org/10.4049/jimmunol.175.11.7437

Kang, X., H.-J. Kim, M. Ramirez, S. Salameh, and X. Ma. 2010. The septic shock-associated IL-10 -1082 A > G polymorphism mediates allele-specific transcription via poly(ADP-Ribose) polymerase 1 in macrophages engulfing apoptotic cells. *J. Immunol.* 184:3718–3724. https://doi.org/10.4049/jimmunol.0903613

Kimmey, J.M., J.P. Huynh, L.A. Weiss, S. Park, A. Kambal, J. Debnath, H.W. Virgin, and C.L. Stallings. 2015. Unique role for ATG5 in neutrophil-mediated immunopathology during *M. tuberculosis* infection. *Nature.* 528:565–569. https://doi.org/10.1038/nature16451

Kopf, M., C. Schneider, and S.P. Nobs. 2015. The development and function of lung-resident macrophages and dendritic cells. *Nat. Immunol.* 16:36–44. https://doi.org/10.1038/ni.3052

Krausgruber, T., K. Blazek, T. Smallie, S. Alzabin, H. Lockstone, N. Sahgal, T. Hussell, M. Feldmann, and I.A. Udalova. 2011. IRF5 promotes inflammatory macrophage polarization and T_H1-T_H17 responses. *Nat. Immunol.* 12:231–238. https://doi.org/10.1038/ni.1990

Lin, C.-C., T.R. Bradstreet, E.A. Schwarzkopf, J. Sim, J.A. Carrero, C. Chou, L.E. Cook, T. Egawa, R. Taneja, T.L. Murphy, et al. 2014. Bhlhe40 controls cytokine production by T cells and is essential for pathogenicity in autoimmune neuroinflammation. *Nat. Commun.* 5:3551. https://doi.org/10.1038/ncomms4551

Lin, C.-C., T.R. Bradstreet, E.A. Schwarzkopf, N.N. Jarjour, C. Chou, A.S. Archambault, J. Sim, B.H. Zinselmeyer, J.A. Carrero, G.F. Wu, et al. 2016. IL-1-induced Bhlhe40 identifies pathogenic T helper cells in a model of autoimmune neuroinflammation. *J. Exp. Med.* 213:251–271. https://doi.org/10.1084/jem.20150568

Machanick, P., and T.L. Bailey. 2011. MEME-ChIP: motif analysis of large DNA datasets. *Bioinformatics.* 27:1696–1697. https://doi.org/10.1093/bioinformatics/btr189

MacMicking, J.D., G.A. Taylor, and J.D. McKinney. 2003. Immune control of tuberculosis by IFN-γ-inducible LRG-47. *Science.* 302:654–659. https://doi.org/10.1126/science.1088063

Maertzdorf, J., M. Ota, D. Repsilber, H.J. Mollenkopf, J. Weiner, P.C. Hill, and S.H.E. Kaufmann. 2011. Functional correlations of pathogenesis-driven gene expression signatures in tuberculosis. *PLoS One.* 6:e26938. https://doi.org/10.1371/journal.pone.0026938

Martínez-Llordella, M., J.H. Esensten, S.L. Bailey-Bucktrout, R.H. Lipsky, A. Marini, J. Chen, M. Mughal, M.P. Mattson, D.D. Taub, and J.A. Bluestone. 2013. CD28-inducible transcription factor DEC1 is required for efficient autoreactive CD4+ T cell response. *J. Exp. Med.* 210:1603–1619. https://doi.org/10.1084/jem.20122387

Maynard, C.L., L.E. Harrington, K.M. Janowski, J.R. Oliver, C.L. Zindl, A.Y. Rudensky, and C.T. Weaver. 2007. Regulatory T cells expressing interleukin 10 develop from Foxp3+ and Foxp3- precursor cells in the absence of interleukin 10. *Nat. Immunol.* 8:931–941. https://doi.org/10.1038/ni1504

McLean, C.Y., D. Bristor, M. Hiller, S.L. Clarke, B.T. Schaar, C.B. Lowe, A.M. Wenger, and G. Bejerano. 2010. GREAT improves functional interpretation of cis-regulatory regions. *Nat. Biotechnol.* 28:495–501. https://doi.org/10.1038/nbt.1630

Moreira-Teixeira, L., P.S. Redford, E. Stavropoulos, N. Ghilardi, C.L. Maynard, C.T. Weaver, A.P. Freitas do Rosário, X. Wu, J. Langhorne, and A. O'Garra. 2017. T Cell-Derived IL-10 Impairs Host Resistance to *Mycobacterium tuberculosis* Infection. *J. Immunol.* 199:613–623. https://doi.org/10.4049/jimmunol.1601340

Murray, P.J., L. Wang, C. Onufryk, R.I. Tepper, and R.A. Young. 1997. T cell-derived IL-10 antagonizes macrophage function in mycobacterial infection. *J. Immunol.* 158:315–321.

Nandi, B., and S.M. Behar. 2011. Regulation of neutrophils by interferon-γ limits lung inflammation during tuberculosis infection. *J. Exp. Med.* 208:2251–2262. https://doi.org/10.1084/jem.20110919

Olobo, J.O., M. Geletu, A. Demissie, T. Eguale, K. Hiwot, G. Aderaye, and S. Britton. 2001. Circulating TNF-α, TGF-β, and IL-10 in tuberculosis patients and healthy contacts. *Scand. J. Immunol.* 53:85–91. https://doi.org/10.1046/j.1365-3083.2001.00844.x

Ow, J.R., Y.H. Tan, Y. Jin, A.G. Bahirvani, and R. Taneja. 2014. Stra13 and Sharp-1, the non-grouchy regulators of development and disease. *Curr. Top. Dev. Biol.* 110:317–338. https://doi.org/10.1016/B978-0-12-405943-6.00009-9

Poon, G.F.T., Y. Dong, K.C. Marshall, A. Arif, C.M. Deeg, M. Dosanjh, and P. Johnson. 2015. Hyaluronan Binding Identifies a Functionally Distinct Alveolar Macrophage-like Population in Bone Marrow-Derived Dendritic Cell Cultures. *J. Immunol.* 195:632–642. https://doi.org/10.4049/jimmunol.1402506

Redford, P.S., A. Boonstra, S. Read, J. Pitt, C. Graham, E. Stavropoulos, G.J. Bancroft, and A. O'Garra. 2010. Enhanced protection to *Mycobacterium tuberculosis* infection in IL-10-deficient mice is accompanied by early and enhanced Th1 responses in the lung. *Eur. J. Immunol.* 40:2200–2210. https://doi.org/10.1002/eji.201040433

Redford, P.S., P.J. Murray, and A. O'Garra. 2011. The role of IL-10 in immune regulation during *M. tuberculosis* infection. *Mucosal Immunol.* 4:261–270. https://doi.org/10.1038/mi.2011.7

Riemann, M., R. Endres, S. Liptay, K. Pfeffer, and R.M. Schmid. 2005. The IkappaB protein Bcl-3 negatively regulates transcription of the IL-10 gene in macrophages. *J. Immunol.* 175:3560–3568. https://doi.org/10.4049/jimmunol.175.6.3560

Roach, D.R., E. Martin, A.G. Bean, D.M. Rennick, H. Briscoe, and W.J. Britton. 2001. Endogenous inhibition of antimycobacterial immunity by IL-10 varies between mycobacterial species. *Scand. J. Immunol.* 54:163–170. https://doi.org/10.1046/j.1365-3083.2001.00952.x

Saraiva, M., and A. O'Garra. 2010. The regulation of IL-10 production by immune cells. *Nat. Rev. Immunol.* 10:170–181. https://doi.org/10.1038/nri2711

Schmidt, E.F., L. Kus, S. Gong, and N. Heintz. 2013. BAC transgenic mice and the GENSAT database of engineered mouse strains. *Cold Spring Harb. Protoc.* 2013:200–206. https://doi.org/10.1101/pdb.top073692

Schreiber, T., S. Ehlers, L. Heitmann, A. Rausch, J. Mages, P.J. Murray, R. Lang, and C. Hölscher. 2009. Autocrine IL-10 induces hallmarks of alternative activation in macrophages and suppresses antituberculosis effector mechanisms without compromising T cell immunity. *J. Immunol.* 183:1301–1312. https://doi.org/10.4049/jimmunol.0803567

St-Pierre, B., G. Flock, E. Zacksenhaus, and S.E. Egan. 2002. Stra13 homodimers repress transcription through class B E-box elements. *J. Biol. Chem.* 277:46544–46551. https://doi.org/10.1074/jbc.M111652200

Sun, H., and R. Taneja. 2000. Stra13 expression is associated with growth arrest and represses transcription through histone deacetylase (HDAC)-dependent and HDAC-independent mechanisms. *Proc. Natl. Acad. Sci. USA.* 97:4058–4063. https://doi.org/10.1073/pnas.070526297

Sun, H., B. Lu, R.Q. Li, R.A. Flavell, and R. Taneja. 2001. Defective T cell activation and autoimmune disorder in Stra13-deficient mice. *Nat. Immunol.* 2:1040–1047. https://doi.org/10.1038/ni721

Turner, J., M. Gonzalez-Juarrero, D.L. Ellis, R.J. Basaraba, A. Kipnis, I.M. Orme, and A.M. Cooper. 2002. *In vivo* IL-10 production reactivates chronic pulmonary tuberculosis in C57BL/6 mice. *J. Immunol.* 169:6343–6351. https://doi.org/10.4049/jimmunol.169.11.6343

Verbon, A., N. Juffermans, S.J. Van Deventer, P. Speelman, H. Van Deutekom, and T. Van Der Poll. 1999. Serum concentrations of cytokines in patients with active tuberculosis (TB) and after treatment. *Clin. Exp. Immunol.* 115:110–113. https://doi.org/10.1046/j.1365-2249.1999.00783.x

Villagra, A., F. Cheng, H.-W. Wang, I. Suarez, M. Glozak, M. Maurin, D. Nguyen, K.L. Wright, P.W. Atadja, K. Bhalla, et al. 2009. The histone deacetylase HDAC11 regulates the expression of interleukin 10 and immune tolerance. *Nat. Immunol.* 10:92–100. https://doi.org/10.1038/ni.1673

Yamada, H., S. Mizuno, M. Reza-Gholizadeh, and I. Sugawara. 2001. Relative importance of NF-kappaB p50 in mycobacterial infection. *Infect. Immun.* 69:7100–7105. https://doi.org/10.1128/IAI.69.11.7100-7105.2001

Yee, C.S.K., Y. Yao, Q. Xu, B. McCarthy, D. Sun-Lin, M. Tone, H. Waldmann, and C.-H. Chang. 2005. Enhanced production of IL-10 by dendritic cells deficient in CIITA. *J. Immunol.* 174:1222–1229. https://doi.org/10.4049/jimmunol.174.3.1222

Zhang, Y., T. Liu, C.A. Meyer, J. Eeckhoute, D.S. Johnson, B.E. Bernstein, C. Nusbaum, R.M. Myers, M. Brown, W. Li, and X.S. Liu. 2008. Model-based analysis of ChIP-Seq (MACS). *Genome Biol.* 9:R137. https://doi.org/10.1186/gb-2008-9-9-r137